IFIC/01-26
FTUV/01-1015
HD-THEP-01-10
FZ-IKP(TH)-01-16

Strangeness-changing scalar form factors

Matthias Jamin[1,*], **José Antonio Oller**[2] **and Antonio Pich**[3]

[1] *Institut für Theoretische Physik, Universität Heidelberg,*
Philosophenweg 16, D-69120 Heidelberg, Germany
[2] *Forschungszentrum Jülich, Institut für Kernphysik (Theorie),*
D-52425 Jülich, Germany
[3] *Departament de Física Teòrica, IFIC, Universitat de València – CSIC,*
Apt. Correus 22085, E-46071 València, Spain

Abstract: We derive expressions for strangeness–changing scalar form factors, which incorporate known theoretical constraints both at low and high energies. Their leading behaviour in the limit of a large number of colours is calculated from the resonance chiral Lagrangian. A set of short-distance constraints on the scalar resonance couplings is obtained, imposing the form factors to vanish at infinite momentum transfer. Making use of previous results on S–wave $K\pi$ scattering [1], and a coupled–channel dispersion–relation analysis, the $K\pi$, $K\eta$ and $K\eta'$ scalar form factors are calculated up to 2 GeV. These scalar form factors are a key ingredient in the determination of the corresponding scalar spectral function which is important in the extraction of the mass of the strange quark from QCD sum rules as well as hadronic τ decays.

PACS: 11.55.Fv, 12.39.Fe, 13.75.Lb, 13.85.Fb
Keywords: Scalar form factors, Chiral Lagrangians, Meson-meson interactions,
Coupled channels, Final state interactions.

[*] Heisenberg fellow.

1 Introduction

QCD currents are a basic ingredient of the electroweak interactions. A good understanding of their associated hadronic matrix elements is required to control the important interplay of QCD in electromagnetic and weak transitions. In this work we shall investigate a simple, although highly non-trivial example of such matrix elements, namely strangeness–changing scalar form factors.

Chiral Perturbation Theory (χPT) [2–7] provides a very powerful framework to study the low-energy dynamics of the lightest pseudoscalar octet. The chiral symmetry constraints are stringent enough to determine the hadronic matrix elements of the light quark currents at very low energies. Unfortunately, these chiral low-energy theorems only apply near threshold. To describe the resonance region around 1 GeV, additional dynamical information is required.

One can construct a chiral–symmetric Effective Field Theory with resonance fields as explicit degrees of freedom [8, 9]. Although not as predictive as the standard chiral Lagrangian for the pseudo-Goldstone mesons, the resonance chiral Lagrangian [8] turns out to provide interesting results, once additional short-distance dynamical QCD constraints are taken into account [9]. At tree level, this Lagrangian encodes the large–N_c properties of QCD [10, 11], in the approximation [12] of keeping only the dominant lowest–mass resonance multiplets.

In the following, we present a detailed analysis of the scalar strangeness–changing form factors, within the resonance chiral framework. These form factors are needed to improve the strange quark mass determination from QCD sum rules for the corresponding scalar current [13–20]. The $\Delta S = 1$ scalar form factors also govern the leading $J = 0$ contributions to the Cabibbo–suppressed hadronic τ decay width. A good theoretical understanding of these quantities could result in a more precise determination of m_s from τ decays [21–26].

In order to work with a renormalisation–group invariant object, we define the scalar form factors $f_X(s)$ from the divergence of the corresponding vector current matrix elements,

$$\langle 0|\partial^\mu(\bar{s}\gamma_\mu u)(0)|X\rangle \;=\; i\,(m_s - m_u)\,\langle 0|(\bar{s}\,u)(0)|X\rangle \;\equiv\; -\,i\,\frac{\Delta_{K\pi}}{\sqrt{2}}\,C_X f_X(s)\,, \qquad (1.1)$$

where $\Delta_{K\pi} \equiv M_K^2 - M_\pi^2$ and $s \equiv p_X^2$. Moreover, we have factored out the normalisation constants C_X, so that $f_X(s) = 1$ at lowest order in χPT. Then the C_X for the lowest lying hadronic systems $K^+\pi^0$, $K^0\pi^+$, $K^+\eta_8$ and $K^+\eta_1$ which contribute to $f_X(s)$ are given by

$$C_{K^+\pi^0} \;=\; 1\,, \qquad C_{K^0\pi^+} \;=\; \sqrt{2}\,, \qquad C_{K^+\eta_8} \;=\; -\frac{1}{\sqrt{3}}\,, \qquad C_{K^+\eta_1} \;=\; 2\sqrt{\frac{2}{3}}\,. \qquad (1.2)$$

Below, we shall only work in the isospin limit with $f_{K\pi} \equiv f_{K^+\pi^0} = f_{K^0\pi^+}$.

The form factors associated with the physical η and η' fields are easily obtained, taking into account the mixing between the two isoscalar states:

$$\begin{pmatrix} \eta \\ \eta' \end{pmatrix} = \begin{pmatrix} \cos\theta & -\sin\theta \\ \sin\theta & \cos\theta \end{pmatrix} \begin{pmatrix} \eta_8 \\ \eta_1 \end{pmatrix} . \tag{1.3}$$

We shall adopt the normalisation $C_{K^+\eta} = C_{K^+\eta_8}$ and $C_{K^+\eta'} = C_{K^+\eta_1}$. Therefore,

$$\begin{aligned} f_{K\eta}(s) &= \cos\theta\, f_{K\eta_8}(s) + 2\sqrt{2}\, \sin\theta\, f_{K\eta_1}(s)\,, \\ f_{K\eta'}(s) &= \cos\theta\, f_{K\eta_1}(s) - \frac{1}{2\sqrt{2}}\, \sin\theta\, f_{K\eta_8}(s)\,. \end{aligned} \tag{1.4}$$

For our numerical analyses we shall use $\sin\theta = -1/3 \approx -20^\circ$, which is in the ball-park of present phenomenological determinations. Notice that for this particular value of the mixing angle $f_{K\eta}(s) = 0$ to lowest order in χPT. Although this cancellation is no longer true at higher orders in the chiral expansion, it indicates a strong suppression of the $K\eta$ current matrix element.

We will first derive the theoretical predictions for $f_X(s)$ in the limit of a large number of colours. This can be achieved in the framework of the resonance chiral Lagrangian. Imposing these form factors to vanish at infinite momentum transfer, we obtain a set of short-distance constraints on the chiral couplings of the scalar meson resonances.

The χPT loops are subleading corrections in the $1/N_c$ counting. They incorporate the unitarity field theory constraints, in a perturbative way, order by order in the momentum expansion. For higher energies around the resonance region and above, the low-energy expansion breaks down because the unitarity corrections due to re-scattering are no longer perturbative. Therefore some kind of resummation of those chiral loops is required to satisfy unitarity [27–38]. This effect appears to be crucial for a correct understanding of the scalar sector, because the S–wave re-scattering of two pseudoscalars is very strong.

In a previous paper [1], we have presented a detailed study of S–wave $K\pi$ scattering up to 2 GeV, within the same resonance chiral framework supplemented with the unitarisation procedure developed in refs. [33, 39]. We will use those results to perform a calculation of the scalar form factors from dispersion relations, explicitly obeying unitarity, also taking into account coupled–channel effects.

In section 2 first the scalar form factors are calculated at tree level in the χPT framework including resonances. Then their expressions in conventional χPT at the next-to-leading order are reviewed and compared to the resonance χPT approach. In section 3 we derive constraints on the scalar form factors by exploiting unitarity and analyticity. These constraints result in a set of coupled dispersion integral equations for the form factors. The

Omnès solution of the dispersion relation in the elastic single channel case is also discussed. Section 4 contains our numerical analysis for the single as well as coupled–channel cases and our central results for the scalar form factors are presented. Finally we close with some conclusions and an outlook in section 5.

2 Effective Lagrangian Results

2.1 Resonance Chiral Lagrangian

In the limit of an infinite number of quark colours, QCD reduces to a theory of tree–level resonance exchanges [10, 11]. At low energies, the dominant effects are governed by the lowest–mass meson multiplets, and can be analysed within the resonance chiral Lagrangian framework developed in refs. [8, 9]. We refer to those references for details on the chiral formalism and notations. We will use a $\mathrm{U}(3)_L \times \mathrm{U}(3)_R$ effective theory with nine pseudoscalar Goldstone bosons, which is the appropriate framework in the limit N_c to infinity [40–42].

The tree–level calculation of the relevant scalar form factors is straightforward. One obtains:

$$\begin{aligned}
f_{K\pi}(s) &= 1 + \frac{4c_m}{f^2}\Big[\, c_d + (c_m - c_d)\,\frac{M_K^2 + M_\pi^2}{M_S^2}\,\Big]\frac{s}{M_S^2 - s}\,, \\
f_{K\eta_8}(s) &= 1 + \frac{4c_m}{f^2(M_S^2 - s)}\Big[\, c_d\Big(s - M_K^2 - p_{\eta_8}^2\Big) + c_m\Big(5M_K^2 - 3M_\pi^2\Big)\,\Big] \\
&\quad + \frac{4c_m(c_m - c_d)}{f^2 M_S^2}\,\Big(3M_K^2 - 5M_\pi^2\Big)\,, \qquad (2.1) \\
f_{K\eta_1}(s) &= 1 + \frac{4c_m}{f^2(M_S^2 - s)}\Big[\, c_d\Big(s - M_K^2 - p_{\eta_1}^2\Big) + c_m\, 2M_K^2\,\Big] - \frac{4c_m(c_m - c_d)}{f^2 M_S^2}\, 2M_\pi^2\,,
\end{aligned}$$

where c_d and c_m are the couplings of the scalar multiplet to the Goldstone bosons, in the lowest–order chiral resonance Lagrangian of refs. [8,9], M_S is the scalar resonance mass and $f \approx f_\pi = 92.4$ MeV is the pion decay constant. The iso-singlet momentum dependence $p_{\eta_i}^2$ refers to the appropriate meson mass squared in the linear combinations (1.4), associated with the physical η and η' fields.

The numerical values of the couplings c_d and c_m are not very well known. We can get a theoretical constraint by enforcing the scalar form factors to vanish at large momentum transfer. This seems a very reasonable phenomenological assumption for a composite object. All three form factors are zero when s goes to infinity, if the following two conditions

are satisfied:

$$4c_d c_m \;=\; f^2\,, \qquad\qquad c_m - c_d \;=\; 0\,. \tag{2.2}$$

This implies

$$c_d \;=\; c_m \;=\; f/2 \;\approx\; 46\ \mathrm{MeV}\,, \tag{2.3}$$

and a dipole structure for the scalar form factors,

$$f_X(s) \;=\; \frac{f_X(0)}{(1-s/M_S^2)}\,. \tag{2.4}$$

Taking $\sin\theta = -1/3$ and $M_S = M_{K_0^*} \approx 1.4$ GeV,

$$\begin{aligned} f_{K\pi}(0) \;&=\; 1\,, \qquad\qquad f_{K\eta}(0) \;=\; 2\sqrt{2}\,\frac{\Delta_{K\pi}}{M_{K_0^*}^2} \;\approx\; 0.33\,, \\ f_{K\eta'}(0) \;&=\; \frac{1}{2\sqrt{2}}\Big[\,3 + \frac{3(M_K^2 - M_{\eta'}^2) + \Delta_{K\pi}}{M_{K_0^*}^2}\,\Big] \;\approx\; 0.74\,. \end{aligned} \tag{2.5}$$

Notice that $f_{K\eta}(0)$ goes to zero in the limit $M_K = M_\pi$.

The above results can easily be generalised to take into account the exchange of N different scalar multiplets with parameters $M_{S,i}$, $c_{d,i}$ and $c_{m,i}$ $(i = 1, \cdots, N)$. In that case, $f_X(s) - 1$ contains a sum of N contributions like the ones in eqs. (2.1), with the appropriate changes on the scalar parameters. The short–distance requirement that $f_X(s)$ goes to zero for $s \to \infty$ then implies the constraints:

$$4\sum_{i=1}^{N} c_{d,i} c_{m,i} \;=\; f^2\,, \qquad\qquad \sum_{i=1}^{N} \frac{c_{m,i}}{M_{S_i}^2}\,(c_{m,i} - c_{d,i}) \;=\; 0\,. \tag{2.6}$$

The consequences of these conditions have already been investigated in the analysis of S–wave $K\pi$ scattering, performed in ref. [1]. A more detailed discussion of the phenomenological implications of the relations (2.6) in the case of two scalar resonances will be given at the end of the next section.

2.2 Chiral Perturbation Theory

The $K\pi$ and $K\eta_8$ scalar form factors have been computed at the one-loop level in $\mathrm{SU}(3)_L \times \mathrm{SU}(3)_R$ χPT [4]. The result can be written as:

$$\begin{aligned} f_{K\pi}(s) \;&=\; 1 + \frac{4L_5^r(\mu)}{f^2}s + \frac{1}{8f^2}\left(5s - 2\Sigma_{K\pi} - 3\frac{\Delta_{K\pi}^2}{s}\right)\bar{J}_{K\pi}(s) \\ &+ \frac{1}{24f^2}\left(3s - 2\Sigma_{K\pi} - \frac{\Delta_{K\pi}^2}{s}\right)\bar{J}_{K\eta_8}(s) + \frac{s}{4\Delta_{K\pi}}\left(5\mu_\pi - 2\mu_K - 3\mu_{\eta_8}\right)\,, \end{aligned} \tag{2.7}$$

$$f_{K\eta_8}(s) \;=\; 3\frac{M_{\eta_8}^2 - M_K^2}{\Delta_{K\pi}}\left\{1 + \frac{4L_5^r(\mu)}{f^2}s + \frac{3}{8f^2}\left(3s - 2\Sigma_{K\pi} - \frac{\Delta_{K\pi}^2}{s}\right)\bar{J}_{K\pi}(s)\right.$$
$$\left. - \frac{1}{24f^2}\left(9s - 2M_K^2 - 18M_{\eta_8}^2 + \frac{\Delta_{K\pi}^2}{s}\right)\bar{J}_{K\eta_8}(s) + \frac{9s}{4\Delta_{K\pi}}\left(\mu_\pi - 2\mu_K + \mu_{\eta_8}\right)\right\}\,, \quad (2.8)$$

where $\Sigma_{K\pi} \equiv M_K^2 + M_\pi^2$.

The unitarity corrections associated with the re-scattering of the final pseudoscalar particles are incorporated through the loop functions $\bar{J}_{PQ}(s)$. Their explicit expressions are given in appendix A. Although the contributions from Goldstone loops are next-to-leading in the $1/N_c$ expansion, they generate large logarithmic corrections to the scalar form factors. The loops introduce a dependence on the renormalisation scale μ in the renormalised chiral coupling $L_5^r(\mu)$ and through the explicit factors

$$\mu_P \;\equiv\; \frac{M_P^2}{32\pi^2 f^2}\ln\left(M_P^2/\mu^2\right). \quad (2.9)$$

Nevertheless, the scalar form factors are of course independent of μ.

In the large–N_c limit, the expressions for the form factors $f_{K\pi}(s)$ and $f_{K\eta_8}(s)$ reduce to

$$f_{K\pi}(s) \;=\; \frac{\Delta_{K\pi}}{3(M_{\eta_8}^2 - M_K^2)}\, f_{K\eta_8}(s) \;=\; 1 + \frac{4L_5 s}{f^2}\,. \quad (2.10)$$

The comparison[1] with the resonance–exchange results in eqs. (2.1) gives the corresponding scalar contribution to the $\mathcal{O}(p^4)$ chiral coupling L_5:

$$L_5^S \;=\; \frac{c_m c_d}{M_S^2} \;\approx\; \frac{f^2}{4M_S^2}\,. \quad (2.11)$$

The resonance propagators appearing in (2.1) provide an explicit resummation of local terms to all orders in the chiral expansion, improving the result (2.10) to the dipole form (2.4). Adding a second scalar resonance with mass $M_{S'}^2$ and couplings c'_d and c'_m, and also taking into consideration the $\mathcal{O}(p^4)$ coupling constant L_8, the contributions from the scalar resonances take the form [8]:

$$L_5^S \;=\; \frac{c_d c_m}{M_S^2} + \frac{c'_d c'_m}{M_{S'}^2} \qquad \text{and} \qquad L_8^S \;=\; \frac{c_m^2}{2M_S^2} + \frac{c_m'^2}{2M_{S'}^2}\,. \quad (2.12)$$

Now, we are in a position to discuss phenomenological consequences of the above relations for the scalar couplings. Using the second of the short–distance constraints (2.6),

[1] The $K\eta_8$ scalar form factor in (2.1) includes an additional term proportional to $c_m c_d \Delta_{K\pi}/M_S^2$, which is generated through η_8–η_1 mixing.

together with the relations (2.12), immediately implies $L_5^S = 2L_8^S$, independent of the number of scalar resonances. Within the uncertainties, this relation is fulfilled by the most recent determination of the chiral couplings L_5 and L_8 [43],

$$L_5 \;=\; (0.91 \pm 0.15) \cdot 10^{-3} \qquad \text{and} \qquad L_8 \;=\; (0.62 \pm 0.20) \cdot 10^{-3}\,, \tag{2.13}$$

suggesting that both the resonance saturation as well as the short–distance constraints are reasonable approximations. However, we only have three linearly independent relations for the four scalar couplings c_d, c_m, c_d' and c_m', so that we have to make further assumptions to obtain estimates for these couplings.

The estimate (2.3) with only one scalar resonance led to $c_d = c_m$ and thus it seems plausible to keep this constraint in addition. One immediate consequence of the constraint and the second relation (2.6) is $c_d' = c_m'$. Employing the first of the short–distance constraints (2.6) and the relations (2.12), the remaining couplings c_d and c_d' can be calculated with the result:

$$c_d \;=\; c_m \;=\; 37.0\ \text{MeV} \qquad \text{and} \qquad c_d' \;=\; c_m' \;=\; 27.7\ \text{MeV}\,. \tag{2.14}$$

Here, the phenomenological value (2.13) for L_5, as well as $M_S = 1.4$ GeV and $M_S' = 1.9$ GeV have been used. The approach of utilising the short–distance constraints, together with $c_d = c_m$ has also been followed in our fit (6.10) of ref. [1]. The fit then resulted in

$$c_d \;=\; c_m \;=\; 23.8\ \text{MeV} \qquad \text{and} \qquad c_d' \;=\; c_m' \;=\; 39.6\ \text{MeV}\,. \tag{2.15}$$

These values would correspond to $L_5^S = 0.72 \cdot 10^{-3}$, which in view of the phenomenological result (2.13) appears a little low, although nevertheless acceptable. One should note that at the tree–level there is some ambiguity in the scalar resonance mass M_S, and e.g. taking $M_S = 1.2$ GeV, eq. (2.14) would change to $c_d = 27.6$ MeV and $c_d' = 37.0$ MeV, much closer to the result (2.15).

A different, although also not implausible assumption would be universality of the chiral couplings, namely $c_d = c_d'$ and $c_m = c_m'$. These constraints allow us to calculate L_5^S from the first of the short–distance relations:

$$L_5^S \;=\; \frac{f^2}{8}\left(\frac{1}{M_S^2} + \frac{1}{M_{S'}^2}\right) \;=\; 0.84 \cdot 10^{-3}\,, \tag{2.16}$$

surprisingly consistent with the phenomenological value (2.13). On the other hand, just using resonance saturation of the chiral couplings (2.12) and their values (2.13), yields

$$c_d \;=\; c_d' \;=\; 29.1\ \text{MeV} \qquad \text{and} \qquad c_m \;=\; c_m' \;=\; 39.7\ \text{MeV}\,, \tag{2.17}$$

which also satisfies the first short–distance relation rather well. However, these parameters violate the second of the short–distance constraints. Enforcing the second constraint in addition again requires $c_d = c_m$, and we fall back to the first assumption. The values of the chiral scalar couplings which correspond to this last scenario are

$$c_d \;=\; c_m \;=\; c_d' \;=\; c_m' \;=\; 32.7\,\mathrm{MeV}\,. \tag{2.18}$$

The ranges of the scalar couplings which arose in the discussion above should give some indication of their present uncertainties which we conclude to be about 30%.

3 Analyticity and unitarity constraints

In this section, we present the formalism employed to calculate the coupled channel $K\pi$, $K\eta$ and $K\eta'$ scalar form factors up to around 2 GeV. The χPT results (2.7) and (2.8) are only valid at low momentum transfers. We have been able to resum the local leading (in $1/N_c$) contributions to all chiral orders, through the resonance propagators. Analyticity and unitarity allow us to obtain further constraints on the scalar form factors. We shall first derive unitarity relations obeyed by the scalar form factors which link these quantities to the S–wave $I = 1/2$ $K\pi$, $K\eta$ and $K\eta'$ partial wave amplitudes. These amplitudes will be taken from our previous work [1], where they were studied in detail up to 2 GeV in the framework of χPT with resonances, supplemented with a suitable unitarisation procedure.

3.1 Unitarity relations

Unitarity of the scattering matrix S immediately implies the following identity for the T–operator,

$$T - T^\dagger \;=\; i\,T\cdot T^\dagger\,, \tag{3.1}$$

where T is defined by $S \equiv 1 + i\,T$. To obtain the form factors in question, the previous general relation is applied to the transition of the states $|K\phi_k\rangle$ (where $\phi_1 = \pi$, $\phi_2 = \eta$ and $\phi_3 = \eta'$) to the vacuum state. The scalar operator giving rise to this transition should have strangeness $|S| = 1$ and isospin $I = 1/2$. Let us remark that we are considering a pure strong interaction problem without electroweak corrections.

Inserting a complete set of intermediate states on the right–hand side of eq. (3.1), and restricting this set to the two–particle states $|K\phi_i\rangle$, we arrive at

$$\langle 0|T|K\phi_k\rangle - \langle 0|T^\dagger|K\phi_k\rangle \;=\; i\sum_i \frac{\theta(s-s_{th\,i})\,q_i(s)}{8\pi\sqrt{s}}\,\langle 0|T|K\phi_i\rangle \int \langle K\phi_i|T^\dagger|K\phi_k\rangle\,d\cos\theta\,, \tag{3.2}$$

where $s = p_i^2$ with p_i being the total four–momentum of the state $|K\phi_i\rangle$, $q_i \equiv \lambda_{K\phi_i}/(2\sqrt{s})$ is the modulus of the centre-of-mass three–momentum for this state, and θ is the corresponding scattering angle. The function $\lambda_{K\phi_i}$ is defined in appendix A, and the trivial centre-of-mass motion has been removed.

Performing a partial wave decomposition of $T^{ik}(s, cos\,\theta) \equiv \langle K\phi_i|T|K\phi_k\rangle$, we have:

$$T^{ik}(s,z) \;=\; 16\pi \sum_{l=0}^{\infty} (2l+1)\, t_l^{ik}(s)\, \mathcal{P}_l(z)\,, \tag{3.3}$$

where $\mathcal{P}_l(z)$ is the Legendre polynomial of degree l with l being the orbital angular momentum and $t_l^{ik}(s)$ are the partial wave amplitudes. Making use of time reversal invariance and inserting the decomposition (3.3) into eq. (3.2), only the S–wave component survives the angular integration. We thus obtain our central unitarity relation for the scalar form factors $F_k(s) \equiv \langle 0|T|K\phi_k\rangle$:

$$\mathrm{Im}\, F_k(s) \;=\; \sum_i \sigma_i(s) F_i(s)\, t_0^{ik}(s)^*\,, \tag{3.4}$$

where, for convenience, we have defined the quantity $\sigma_i(s) \equiv \theta(s - s_{th\,i})\, 2q_i(s)/\sqrt{s}$. For an appropriate choice of the scalar T–operator with isospin 1/2, in accordance with eq. (1.1), the form factors $F_k(s)$ are related to $f_X(s)$ of section 1 by:

$$F_{K\pi}(s) \;=\; f_{K\pi}(s)\,, \qquad F_{K\eta}(s) \;=\; \frac{C_{K\eta}}{\sqrt{3}}\, f_{K\eta}(s)\,, \qquad F_{K\eta'}(s) \;=\; \frac{C_{K\eta'}}{\sqrt{3}}\, f_{K\eta'}(s)\,. \tag{3.5}$$

We use an isospin basis of states $|K\phi_k\rangle$. The coupling of the $|K\pi\rangle$ state with $I = I_3 = 1/2$ to the scalar current in (1.1) is a factor $\sqrt{3}$ larger than the one of $|K^+\pi^0\rangle$. Too keep the same normalisation as for $f_{K^+\pi^0}(s)$, we rescale all form factors by a global factor $1/\sqrt{3}$.

As stated above, the sum in eq. (3.4) is restricted to two–particle intermediate states. Thus some comments about the role of multiparticle states are in order. The lightest multiparticle state contributing to this sum is $|K\pi\pi\pi\rangle$. From the theoretical side, its contributions are suppressed both in the chiral and large–N_c expansions. Experimentally, in [44, 45] it has been established that the $I = 1/2$ S–wave $K\pi$ amplitude is elastic below roughly 1.3 GeV with $K\eta'$ being the first relevant inelastic channel. These conclusions have been confirmed in [1] where it was demonstrated that the contribution of the $K\eta$ channel to the S–wave amplitude could be neglected. However, it was also found in this work that for energies higher than about 2 GeV other inelastic channels become increasingly important.

The unitarity relation (3.4) given above poses tight constraints on the scalar form factors. For the elastic case one simply has:

$$\mathrm{Im}\, F_1(s) \;=\; \sigma_1(s) F_1(s)\, t_0^{11}(s)^* \tag{3.6}$$

which implies the well known Watson final state theorem [46], stating that the phase of $F_1(s)$ is the same as the one of $t_0^{11}(s)$. This is obvious from the previous equation since its left–hand side is real.

Let us now discuss the two–channel case, which is very appropriate since the contributions from the $K\eta$ state are negligible to a very good approximation. Substituting $\mathrm{Im}\, F_k(s)$ by $(F_k(s) - F_k(s)^*)/2i$ in eq.(3.4), one finds above the threshold of the $K\eta'$:

$$F_1(s) = \Big(1 + 2i\,\sigma_1(s)\,t_0^{11}(s)\Big)F_1(s)^* + 2i\,\sigma_3(s)\,t_0^{13}(s)\,F_3(s)^*\,, \tag{3.7}$$

$$F_3(s) = 2i\,\sigma_1(s)\,t_0^{13}(s)\,F_1(s)^* + \Big(1 + 2i\,\sigma_3(s)\,t_0^{33}(s)\Big)F_3(s)^*\,, \tag{3.8}$$

where, although working with two channels, we have used the label 3 to indicate the $K\eta'$ state as introduced before. Following ref. [47], we now express $F_3(s)$ in terms of $F_1(s)$ from eqs. (3.7) and (3.8).

The partial wave amplitudes t_0^{mn} can be parametrised by introducing the symmetric and unitary 2×2 S–matrix $S_{mn} = \delta_{mn} + 2i\sqrt{\sigma_m \sigma_n}\, t_0^{mn}$:

$$S = \begin{pmatrix} \eta\, \exp 2i\delta_1(s) & i\sqrt{1-\eta^2}\exp i(\delta_1(s) + \delta_3(s)) \\ i\sqrt{1-\eta^2}\exp i(\delta_1(s) + \delta_3(s)) & \eta\, \exp 2i\delta_3(s) \end{pmatrix} \tag{3.9}$$

with $\eta \equiv \cos 2\alpha$ ($\sin 2\alpha = \sqrt{1-\eta^2}$) the inelasticity parameter ($0 \le \eta \le 1$) and $\delta_k(s)$ the phase shift of channel k. We further express the form factors as $F_k(s) = f_k \exp i(\delta_k + \phi_k)$ with f_k and ϕ_k real functions and $f_k \ge 0$. Taking real and imaginary parts in eqs. (3.7) and (3.8), the following set of relations emerges:

$$(1 - \cos 2\alpha)\cos\phi_1 f_1 = \sqrt{\frac{\sigma_3}{\sigma_1}}\,\sin 2\alpha\,\sin\phi_3 f_3\,, \tag{3.10}$$

$$(1 + \cos 2\alpha)\sin\phi_1 f_1 = \sqrt{\frac{\sigma_3}{\sigma_1}}\,\sin 2\alpha\,\cos\phi_3 f_3\,; \tag{3.11}$$

plus two analogous relations with the labels 1 and 3 exchanged. The latter relations are, however, linearly dependent to the first two. Dividing the two eqs. (3.10) and (3.11) results in:

$$\tan\phi_1 \tan\phi_3 = \tan^2\alpha\,, \tag{3.12}$$

whereas adding them in quadrature yields:

$$\frac{\sigma_3 f_3^2}{\sigma_1 f_1^2} = \tan^2\alpha + (\cot^2\alpha - \tan^2\alpha)\sin^2\phi_1\,. \tag{3.13}$$

Thus, once f_1 and ϕ_1 are known, f_3 and ϕ_3 can be calculated from eqs. (3.12) and (3.13). The treatment in the full three–channel case will be discussed further below.

3.2 Dispersion relations

The scalar form factors $F_k(s)$ are analytic functions in the complex s–plane, except for a cut along the positive real axis, starting at the first physical threshold $s_{th\,1} = (M_K + M_\pi)^2$, where their imaginary parts develop discontinuities. They are real for $s < s_{th\,1}$. As should be clear from eq. (3.4), their imaginary parts just correspond to the contributions from all possible on-shell intermediate states.[2]

Analyticity relates the real and imaginary parts of $F_k(s)$ through dispersion relations:

$$F_k(s) \;=\; \frac{1}{\pi}\int\limits_{s_{th\,1}}^{\infty} ds'\,\frac{\mathrm{Im}F_k(s')}{(s'-s-i0)} + \text{subtractions}\,. \tag{3.14}$$

From unitarity, as shown above, $\mathrm{Im}F_k(s)$ takes the form of eq. (3.4). With the reasonable assumption that for s going to infinity, $F_k(s)$ vanishes sufficiently fast, the form factors satisfy dispersion relations without subtractions. This assumption was already explored in section 2.

Because $K\pi$ scattering is basically elastic up to around 1.3 GeV, it is again instructive to consider the single channel case. Then the dispersion relation takes the form:

$$F_1(s) \;=\; \frac{1}{\pi}\int\limits_{s_{th\,1}}^{\infty} ds'\,\frac{\sigma_1(s')F_1(s')\,t_0^{11}(s')^*}{(s'-s-i0)}\,. \tag{3.15}$$

In this case the partial wave amplitude can be expressed as $\sigma_1 t_0^{11} = \sin\delta_1 \exp(i\delta_1)$, and the previous eq. (3.15) admits the well known Omnès–exponential solution [48]:

$$F_1(s) \;=\; P(s)\exp\left(\frac{s}{\pi}\int\limits_{s_{th\,1}}^{\infty} ds'\,\frac{\delta_1(s')}{s'(s'-s-i0)}\right)\,, \tag{3.16}$$

with $P(s)$ being a real polynomial to take care of the zeros of $F_1(s)$ for finite s and $\delta_1(s)$ is the S–wave $I = 1/2$ elastic $K\pi$ phase shift.

In writing eq. (3.16), we have included one subtraction at the origin since generally $\delta_1(s)$ tends to a constant for s going to infinity. A general solution, valid for any number n of subtractions at an arbitrary subtraction point s_0, has been given in refs. [30, 49], where the equivalence of the different expressions has been discussed in detail. The form factor $F_1(s)$ in the elastic case will be discussed further in our numerical analysis below.

In order to implement the dispersion relation for coupled channels, we neglect, for the moment, the $K\eta$ contribution and only consider the more important $K\pi$ and $K\eta'$ channels.

[2] We are excluding the presence of bound state poles below the threshold of the $K\pi$ state.

For this case, two coupled integral equations arise:

$$
\begin{aligned}
F_1(s) &= \frac{1}{\pi}\int\limits_{s_{th\,1}}^{\infty} ds'\,\frac{\sigma_1(s')F_1(s')\,t_0^{11}(s')^*}{(s'-s-i0)} + \frac{1}{\pi}\int\limits_{s_{th\,3}}^{\infty} ds'\,\frac{\sigma_3(s')F_3(s')\,t_0^{13}(s')^*}{(s'-s-i0)}\,, \\
F_3(s) &= \frac{1}{\pi}\int\limits_{s_{th\,1}}^{\infty} ds'\,\frac{\sigma_1(s')F_1(s')\,t_0^{13}(s')^*}{(s'-s-i0)} + \frac{1}{\pi}\int\limits_{s_{th\,3}}^{\infty} ds'\,\frac{\sigma_3(s')F_3(s')\,t_0^{33}(s')^*}{(s'-s-i0)}\,. \qquad (3.17)
\end{aligned}
$$

The integral equations (3.17) will be solved iteratively according to a procedure already applied in ref. [50]. In the first step initial functions $F_k^{(0)}(s)$ for the form factors, to be specified further below, are inserted in the right–hand side of eqs. (3.17), and new resulting form factors $F_k^{(1)}(s)$ are calculated. Then the procedure is iterated until after n steps the procedure converges and the final scalar form factors $F_k^{(n)}(s)$ are obtained.

The dispersion relations for the three–channel case including the $K\eta$ contribution are completely analogous to the eqs. (3.17). Thus the explicit expressions have been relegated to appendix B. As for the two–channel case, they are solved iteratively. Further details on the numerical methods will be given in the next section below.

4 Numerical analysis

In this section we present the different solutions to the dispersion relations of eqs. (3.15), (3.17) and (B.1) for the scalar $K\pi$, $K\eta$ and $K\eta'$ form factors. The required partial wave amplitudes are taken from our previous work [1]. First, we investigate the single channel elastic case for which the analytical Omnès solution is available. Then the inelastic two– and three–channel problems are treated for which we have to resort to numerical methods.

4.1 Elastic $K\pi$ channel

In the elastic case, the analytical Omnès solution is given by eq. (3.16). It only depends on the elastic $K\pi$ phase shift $\delta_1(s)$. However, we still have to fix the polynomial ambiguity $P(s)$. This can be achieved from the assumption that $F_1(s)$ should vanish for s going to infinity.

Investigating $F_1(s)$ in this limit, from eq. (3.16) one finds:

$$
\lim_{s\to\infty} F_1(s) \;=\; e^{i\delta_{1\infty}} \lim_{s\to\infty} P(s)\Big(\frac{s_{th\,1}}{s}\Big)^{\delta_{1\infty}/\pi}\,, \qquad (4.1)
$$

with $\delta_{1\infty} \equiv \lim_{s\to\infty}\delta_1(s)$. In the single channel case with one resonance, $\delta_{1\infty}$ is expected to be equal to π [51]. Assuming $F_1(s)$ to vanish at infinity thus requires that $P(s)$ should

be constant. This constant can be determined from the normalisation of $F_1(s)$ at $s = 0$. Then the Omnès formula takes the form:

$$F_1(s) \;=\; F_1(0) \exp\left(\frac{s}{\pi} \int\limits_{s_{th\,1}}^{\infty} ds' \, \frac{\delta_1(s')}{s'(s'-s-i0)}\right) . \tag{4.2}$$

In our numerical analysis, for $F_1(0)$ we will use the next-to-leading order χPT result of eq. (2.7), namely $F_1^{\chi\mathrm{PT}}(0) = f_{K\pi}(0) = 0.981$. This is very close to the leading order value 1, demonstrating that at $s = 0$, as expected, χPT works extremely well.

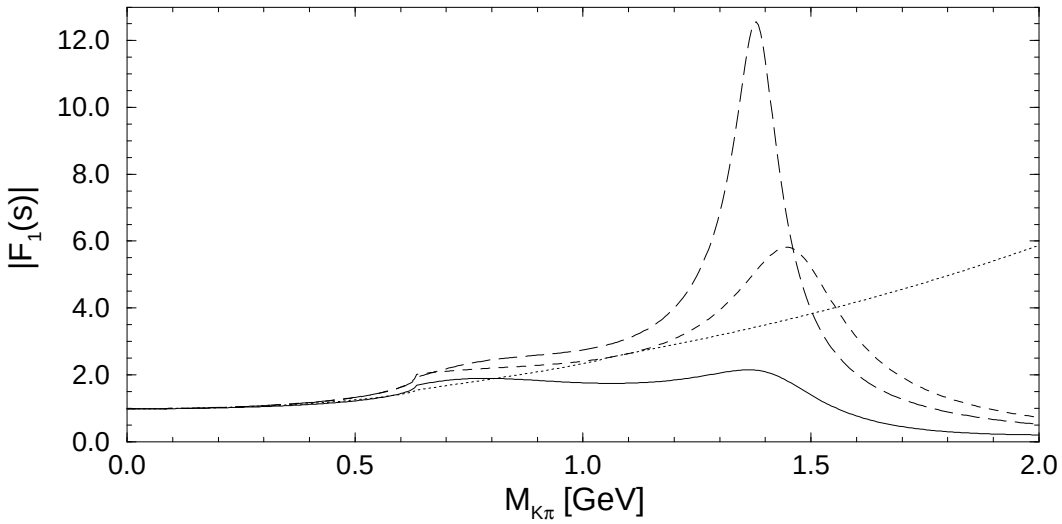

Figure 1: $|F_1(s)|$ in the elastic case. Long–dashed line: χPT fit of eq. (4.9) of [1]; solid line: χPT fit of eq. (4.10) of [1]; short–dashed line: K-matrix fit of eq. (4.13) of [1]; dotted line: next-to-leading order χPT result of eq. (2.7).

Inputs for the phase shift $\delta_1(s)$, required in eq. (4.2), will be taken from different fits of our previous work on S–wave $K\pi$ scattering [1]. In fig. 1 the absolute value of the form factor, $|F_1(s)|$, is displayed for three different elastic fits, as a function of the invariant mass of the $K\pi$ system $M_{K\pi} = \sqrt{s}$. The long–dashed line corresponds to the χPT fit of eq. (4.9) of [1], the solid line to the χPT fit of eq. (4.10) of [1], and finally the short–dashed line corresponds to the K-matrix fit of eq. (4.13) of [1]. For comparison, as the dotted line we also show the next-to-leading order χPT result of eq. (2.7). This comparison shows that up to the $K\pi$ threshold region, next-to-leading order χPT gives a good description of the scalar form factor.

As is obvious from fig. 1, although all three fits give very good representations of the $K\pi$ scattering data in the elastic region, the corresponding form factors, especially in the resonance region, behave very differently. Let us discuss these findings in more detail. In

the resonance region the form factor corresponding to our best elastic fit of eq. (4.10) of [1] is almost flat, displaying no significant resonance structure. This can be traced back to the fact that for large s, $\delta_1^{(4.10)}(s)$ tends to zero, whereas for the passage of one resonance the phase shift should go to π. The χPT fit of eq. (4.9) of [1], including the short–distance constraint discussed in section 2, on the other hand, displays this behaviour. However, in this case the scalar form factor in the resonance region is rather large. This is due to the fact that for this fit the width of the $K_0^*(1430)$ comes out to be very small, about a factor of three below the experimental average. (See section 7 of [1].) Nevertheless, one has to strongly stress that a proper study of the resonance region can only be performed after including the $K\eta'$ with a threshold around 1.45 GeV, as shown below.

With respect to the general behaviour discussed above, the form factor corresponding to the K-matrix fit of eq. (4.13) of [1] appears to be the most realistic one. $\delta_1^{(4.13)}(s)$ tends to π for large s and also the resonance parameters of the $K_0^*(1430)$ for this fit are close to the experimental average. The K-matrix fit is also different from the chiral fits because the corresponding ansatz for the partial wave amplitude is free of left–hand cuts. In this case it is even possible to give a closed expression for the form factor [47, 51]:

$$F_1(s) \;=\; \prod_{i,j} \frac{(1 - s/s_{p_i})}{(1 - s/s_{z_j})} \, \frac{F_1(0)}{\Big(1 - C(s) K_0^{1/2}(s)\Big)} \,, \tag{4.3}$$

where $C(s) = 16\pi \bar{J}_{K\pi}(s)$ and the explicit expression for the K-matrix ansatz $K_0^{1/2}(s)$ is given in eq. (4.12) of [1]. The s_{p_i} and s_{z_i} are the locations of the poles and zeros of $(1 - C(s)K(s))^{-1}$ which have to be removed in the form factor. In our particular case we have one pole at $s_{p_1} = -2.011\,\mathrm{GeV}^2$ and two zeros at $s_{z_1} = -5.821\,\mathrm{GeV}^2$ and $s_{z_2} = M^2_{K_0^*(1430)}$. It is an easy matter to verify that the representation (4.3) yields the same scalar form factor as the Omnès formula (4.2).

4.2 The two–channel case

We now turn to the two–channel case, for which the important effects of the $K\eta'$ are considered in the coupled channel integral equations (3.17). Let us first briefly describe our numerical treatment of these integral equations.

The first step consists in rewriting the coupled integral equations according to the procedure described in appendix C.1. As central values for the two parameters which are introduced in this context we take $s_{cut} = 9\ \mathrm{GeV}^2$ and $b = -0.8$. We have, however, varied these parameters to test the numerical stability of our approach.[3] Next, the resulting

[3] One of us, J.A.O., has implemented a different numerical approach, finding agreement for the resulting

integral equations are solved iteratively according to a procedure already employed in ref. [50].

For the iterative solution we require initial functions $F_1^{(0)}(s)$ and $F_3^{(0)}(s)$. For $F_1^{(0)}(s)$, we use the form factor which results from employing the Omnès formula (4.2). The phase-shift $\delta_1(s)$ is taken according to the decomposition (3.9). As a starting point, the form factor $F_3^{(0)}(s)$ can be set to zero. We have verified that other initial choices for this function lead to the same final form factors.

Since the dispersion integrals are calculated according to the principal value prescription, the immediate results of our first iteration step are the real parts $\mathrm{Re}F_1^{(1)}(s)$ and $\mathrm{Re}F_3^{(1)}(s)$. From these results, together with the initial imaginary parts $\mathrm{Im}F_1^{(0)}$ and $\mathrm{Im}F_3^{(0)}$, and making use of the central unitarity relation (3.4), the new full form factors $F_1^{(1)}$ and $F_3^{(1)}$ are obtained. This procedure is repeated, until after n steps it has converged reasonably well and the final form factors $F_1^{(n)}$ and $F_3^{(n)}$ can be extracted.

In what follows, we shall explicitly investigate the form factors corresponding to the two–channel fits (6.10) and (6.11) of ref. [1] to the S–wave $K\pi$-scattering data. In a forthcoming publication [52], these form factors and the corresponding scalar spectral function will be utilised to calculate the mass of the strange quark in the framework of QCD sum rules.

The absolute value of the resulting inelastic two–channel $K\pi$ and $K\eta'$ form factors $F_1(s)$ and $F_3(s)$ is displayed in figures 2 and 3. The solid line corresponds to the χPT fit of eq. (6.10) of ref. [1] and the long–dashed line to the fit (6.11). Depending on the high-energy behaviour of the phase shifts $\delta_1(s)$ and $\delta_3(s)$, the dispersion relations admit one or two linearly independent solutions [47]. For the fits (6.10) and (6.11), with s going to infinity, $\delta_1(s)$ tends to π whereas $\delta_3(s)$ tends to zero. In this case there is only one solution to the two–channel dispersion relation. However, we still have the freedom to normalise both solutions $F_1(s)$ and $F_3(s)$ by a common factor. We have used this freedom to again fix $F_1^{\chi\mathrm{PT}}(0) = f_{K\pi}(0) = 0.981$.

The value of the $K\eta'$ form factor at zero momentum is then determined and we obtain $F_3^{(6.10)}(0) = 0.430$ and $F_3^{(6.11)}(0) = 0.409$. These results should be compared with the tree–level expectation from $\mathrm{U}(3)_L \times \mathrm{U}(3)_R$ χPT in the large-N_c limit including resonances of eq. (2.5), $F_3^{\chi\mathrm{PT}}(0) = 2\sqrt{2}/3 f_{K\eta'}(0) = 0.696$. We observe that the resulting value for $F_3(0)$ from the solution of the coupled channel dispersion relation turns out to be somewhat lower than the tree–level result. We shall come back to a discussion of this point below.

For comparison, as the dotted line in figure 2, we have displayed the form factor that

form factors.

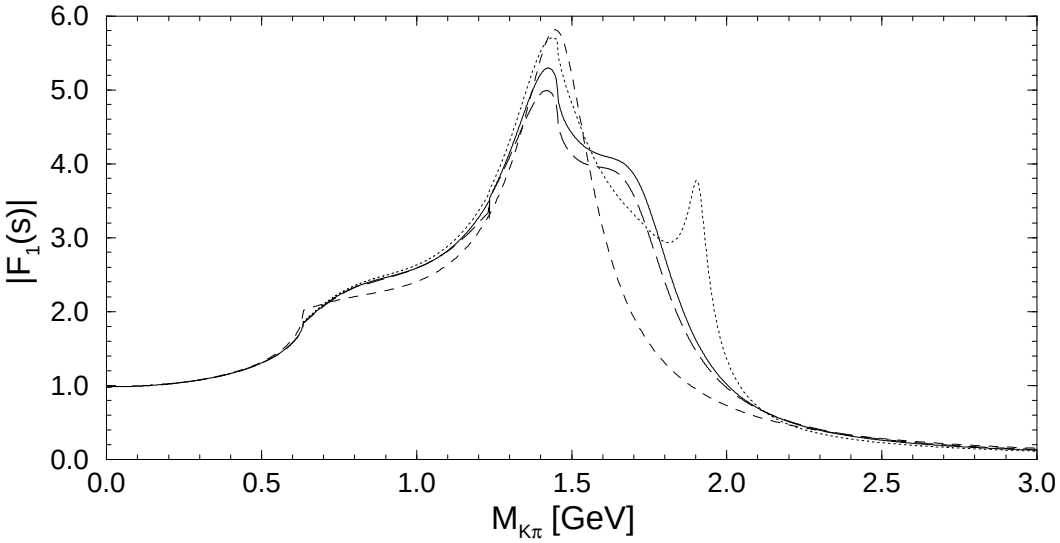

Figure 2: $|F_1(s)|$ in the two–channel case. The solid and long–dashed lines correspond to the χPT fits of eqs. (6.10) and (6.11) of [1] respectively. For comparison, the elastic K-matrix fit of eq. (4.13) is displayed as the short–dashed line, and the dotted line represents the Omnès formula (4.2), evaluated with $\delta_1^{(6.10)}(s)$.

results from evaluating the Omnès formula eq. (4.2) with $\delta_1^{(6.10)}(s)$. $F_1^{\rm Omnès}(s)$ has been used as the starting point for the iteration of the integral equations. From figure 2 it is clear that, apart from the region of the second resonance, the Omnès representation of $F_1(s)$ already gives a reasonable description of this form factor. In addition, as the short–dashed line in figure 2 we have also plotted $|F_1(s)|$ corresponding to the elastic K-matrix fit of eq. (4.13) of [1]. Here we observe that the corresponding form factor behaves rather differently in the $K\pi$ threshold region. This should come as no surprise, because as has been already discussed at the end of section 4 of ref. [1], also the scattering lengths for this fit come out very different compared to χPT.

As was already mentioned above, for the fits (6.10) and (6.11) the total phase motion of $\delta_1(s) + \delta_3(s)$ for s going to infinity only reaches π, whereas on general grounds for two resonances it is expected to approach 2π. The reason for this behaviour of our unitarised chiral fits can be traced back to a deficient description of the experimental data [45] above roughly 1.9 GeV. To improve the description in the region of the second resonance and above, we have performed new fits with a K-matrix ansatz. In the fitting process, the K-matrix ansatz is matched smoothly to the chiral fits at an energy around 1.75 GeV.

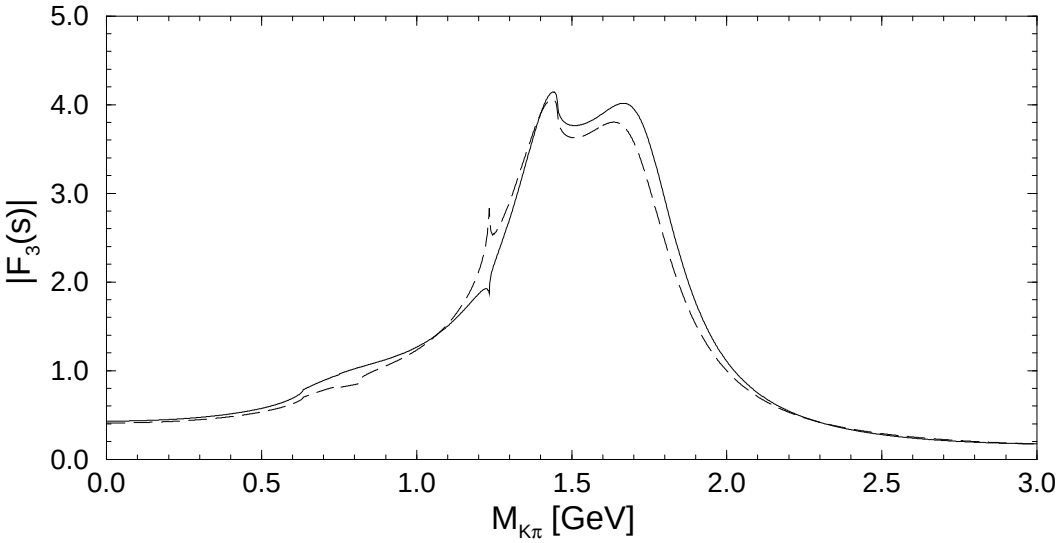

Figure 3: $|F_3(s)|$ in the two–channel case. The solid and long–dashed lines correspond to the χPT fits of eqs. (6.10) and (6.11) of [1] respectively.

For the K-matrix we use a resonance plus background parametrisation:

$$K_{ij}(s) \;=\; \frac{r_i r_j}{(M_{S'}^2 - s)} + \frac{(a_{ij} + b_{ij} s)}{[1 + (s/c)^\kappa]}\,, \tag{4.4}$$

with $\kappa = 0$, 1 if $b_{ij} = 0$ and $\kappa = 2$ otherwise. Except for the first case $\kappa = 0$, this K-matrix is constructed such that it vanishes linearly at large s, and above 1.75 GeV it replaces the matrix $N(s)$ in eq. (6.1) of ref. [1]. Because of time-reversal invariance, $K(s)$ has to be symmetric. Above 1.75 GeV, we then fit this ansatz to the data set A of [45] which extends up to 2.52 GeV. Simultaneously a smooth matching to either one of the unitarised chiral fits (6.10) or (6.11) of [1] at around 1.75 GeV is imposed in the fitting procedure as well. To judge the dependence of the K-matrix fits on the background parametrisation, we have actually calculated four different types of fits. All fits have been performed with the program Minuit [53], and the parameters of these fits are compiled in table 1. As examples, in figure 4 we display the experimental $K\pi$ scattering data of refs. [44, 45], together with the unitarised chiral fit (6.10) of [1] (solid line) and the new K-matrix fits with improved behaviour in the region of the second resonance (6.10K1) (dashed-dotted line) and (6.10K4) (dotted line). The corresponding curves for the other fits look very similar.

For the first type of fits (6.10K1) and (6.11K1), as the background we have just taken constants a_{ij}. This entails that the T-matrix at large s does only fall off as $1/\ln(s)$, and that the total phase motion at infinity, $\delta_{1\infty} + \delta_{3\infty}$ is only π, analogous to the case of the unitarised chiral fits. For the convenience of the reader, the separate phases at infinity, $\delta_{1\infty}$

Fit	(6.10K1)	(6.10K2)	(6.10K3)	(6.10K4)	(6.11K1)	(6.11K2)	(6.11K3)	(6.11K4)
M'_S [GeV]	2.040	2.040	1.904	1.909	1.837	1.837	1.838	1.837
r_1 [GeV]	1.007	1.003	0.567	0.617	0.495	0.501	0.449	0.433
r_2 [GeV]	1.420	1.406	0.550	0.648	0.595	0.603	0.499	0.474
a_{11}	−0.723	−0.801	−0.703	0.221	−0.350	−0.407	−0.647	−0.346
a_{12}	−0.905	−0.990	0.495	1.797	−0.356	−0.415	0.565	1.741
a_{22}	−1.450	−1.580	−1.276	−0.159	−0.567	−0.656	−0.390	0.750
b_{11} [GeV^{-2}]	0	0	0.106	−0.308	0	0	0.145	0.028
b_{12} [GeV^{-2}]	0	0	−0.214	−0.738	0	0	−0.224	−0.606
b_{22} [GeV^{-2}]	0	0	0.366	−0.123	0	0	0.055	−0.326
c [GeV^2]	∞	25	25	4	∞	25	25	4
χ^2/33 dof	74.9	75.5	42.3	45.2	83.3	87.4	43.2	38.0
$\delta_{1\infty}$, $\delta_{3\infty}$	π, 0	π, π	2π, 0	2π, 0	π, 0	π, π	π, π	2π, 0

Table 1: Different K-matrix fits corresponding to the fits (6.10) and (6.11) of [1] in the region above 1.75 GeV. For a detailed discussion see the text.

and $\delta_{3\infty}$, have also been collected in table 1. For these two fits, again $F_3(0)$ is determined, and comes out as $F_3^{(6.10K1)}(0) = 0.591$ and $F_3^{(6.11K1)}(0) = 0.574$ for (6.10K1) and (6.11K1) respectively, much closer to the tree-level result $F_3^{\chi\rm PT}(0) = 0.696$. As was already remarked above, at the tree–level the scalar resonance mass M_S has some ambiguity, and e.g. using $M_S = 1.2$ GeV in eq. (2.5) would yield $F_3^{\chi\rm PT}(0) = 0.586$, in perfect agreement with the fit results for $F_3(0)$.

To further investigate the quality of our fits, in the following we shall include additional low-energy constraints on the scalar $K\pi$ form factor which come from pure next-to-leading order χPT [4]. Rather precise information on $F_1(s)$ is available at the so called Callan-Treiman point $M_K^2 - M_\pi^2$, because at that point $F_1(\Delta_{K\pi})$ only differs from F_K/F_π by terms of order m_u or m_d,

$$F_1(\Delta_{K\pi}) \;=\; \frac{F_K}{F_\pi} + \Delta_{CT}\,, \tag{4.5}$$

where numerically $\Delta_{CT} = -3.0 \cdot 10^{-3}$ at the next-to-leading order in χPT, and the analytic expression can be found in the second of refs. [4]. Taking most recent values for the decay constants F_K and F_π from [54], we conclude that $F_1(\Delta_{K\pi}) = 1.22 \pm 0.01$.

Furthermore, from χPT we also have information on the slope of the $K\pi$ form factor at zero energy, $D_1(0) \equiv F_1'(0)/F_1(0)$. In χPT at the next-to-leading order, one obtains $D_1(0) = 0.873$ GeV^{-2}, where the uncertainty due to higher order corrections was estimated

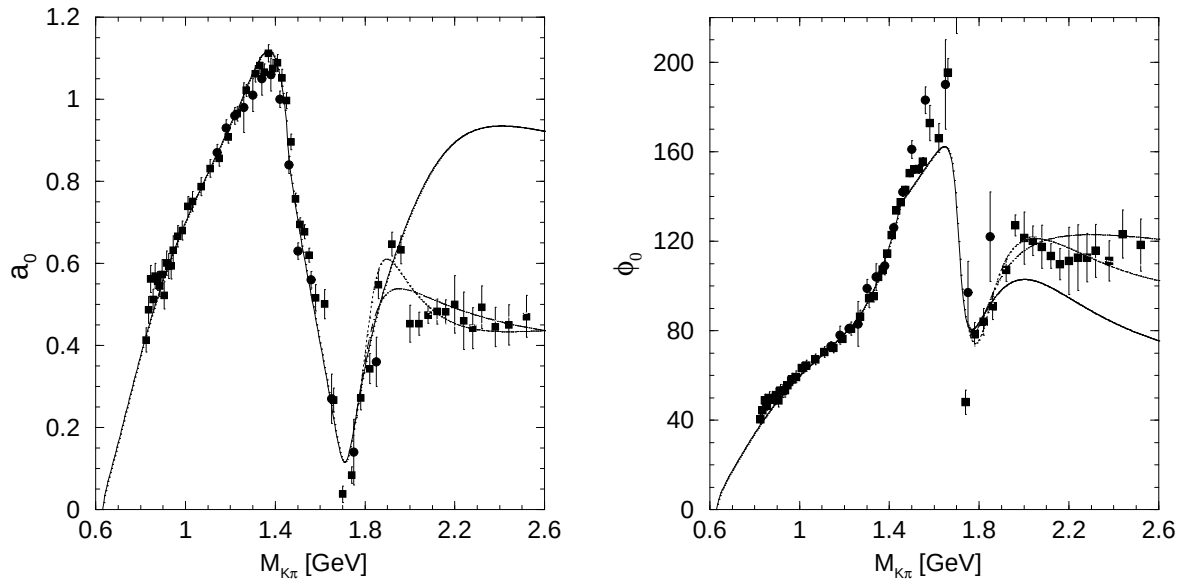

Figure 4: Two-channel fits for a_0 and ϕ_0. The experimental data are given by: solution B of [44] full circles; solution A of [45] full squares. The solid line represents our unitarised chiral fit (6.10) of ref. [1], and, as examples, the dashed-dotted and dotted lines show the new K-matrix fits (6.10K1) and (6.10K4) respectively, which display an improved behaviour in the region of the second resonance.

to be around 20% [4]. This value can also be compared to experimental data. The slope of the scalar form factor has been measured in charged as well as neutral Kaon decays, with the results $\lambda_0 = 0.006 \pm 0.007$ and $\lambda_0 = 0.025 \pm 0.006$ respectively [54]. Here, the parameter λ_0 is defined by $\lambda_0 \equiv D_1(0) M_\pi^2$. Taking the average of the experimental results and enlarging the error according to the standard procedure of the Particle Data Group for inconsistent measurements, we obtain $\lambda_0 = 0.017 \pm 0.009$, whereas from the χPT result together with the isospin average $M_\pi = 138$ MeV, we also find $\lambda_0 = 0.017$, displaying complete agreement for the central results.

Let us now compare $D_1(0)$ and especially $F_1(\Delta_{K\pi})$ with the numbers emerging from our fits. For the K-matrix fits which accomplish a good description of the high energy data above 1.75 GeV, we get $F_1^{(6.10K1)}(\Delta_{K\pi}) = 1.220$ and $F_1^{(6.11K1)}(\Delta_{K\pi}) = 1.219$, in impressive agreement with the precise χPT expectation of eq. (4.5). In addition, the slope is found to be $D_1^{(6.10K1)}(0) = 0.894$ GeV^{-2} as well as $D_1^{(6.11K1)}(0) = 0.893$ GeV^{-2}, also very close to the χPT value. On the other hand, for the original unitarised chiral fits the corresponding results are $F_1^{(6.10)}(\Delta_{K\pi}) = 1.262$ and $F_1^{(6.11)}(\Delta_{K\pi}) = 1.260$, as well as $D_1^{(6.10)}(0) = 0.918$ GeV^{-2} and $D_1^{(6.11)}(0) = 0.909$ GeV^{-2}. Although the values for $D_1(0)$

are compatible with our previous results, $F_1(\Delta_{K\pi})$ turns out too large for both fits, again reflecting an insufficient description of the higher energy region for these fits.

$F_1(\Delta_{K\pi})$	$F_3(0)$	$D_1(0)$ [GeV^{-2}]	$F_1(\Delta_{K\pi})$	$F_3(0)$	$D_1(0)$ [GeV^{-2}]
	(6.10K2)			(6.11K2)	
1.21	0.636	0.848	1.21	0.612	0.850
1.22	0.587	0.863	1.22	0.565	0.866
1.23	0.538	0.879	1.23	0.518	0.882
	(6.10K3)			(6.11K3)	
1.21	0.586	0.828	1.21	0.618	0.777
1.22	0.567	0.851	1.22	0.587	0.805
1.23	0.547	0.874	1.23	0.556	0.834
	(6.10K4)			(6.11K4)	
1.21	0.622	0.851	1.21	0.615	0.858
1.22	0.590	0.868	1.22	0.579	0.874
1.23	0.557	0.886	1.23	0.544	0.890

Table 2: $F_3(0)$ and $D_1(0)$ for the unitarised chiral plus K-matrix fits (6.10K2–4) and (6.11K2–4) with $\delta_{1\infty} + \delta_{3\infty} = 2\pi$, chosen such that $F_1(\Delta_{K\pi}) = 1.22 \pm 0.01$.

For the previous fits, the total phase motion $\delta_{1\infty} + \delta_{3\infty}$ was only π, although for two resonances 2π would be expected. The differences are due to the background accompanying the bare K-matrix poles in eq. (4.4). The latter behaviour can be achieved by forcing the K-matrix to vanish at infinity as will be implemented in all our remaining fits. In this way, we also test the stability of our results under changes in the parameterisations that induce different T-matrices well above the second resonance region around 2 GeV. As a first step, in the fits (6.10K2) and (6.11K2), we introduce an additional cutoff parameter $c = 25$ GeV^2. As long as c is large enough, the sensitivity on this parameter is rather small and it cannot be incorporated as a fit parameter. As can be seen from table 1, the remaining fit parameters do depend only little on this modification. Nevertheless, now both phase shifts δ_1 and δ_3 approach π at infinity. As a consequence, the dispersion relations (3.17) admit two linearly independent solutions. Thus, besides $F_1(0)$, now we are in a position to also fix $F_3(0)$ as an initial condition. In our opinion the best information available is $F_1(\Delta_{K\pi})$, and therefore we fix $F_3(0)$ such as to fullfill the constraint on this quantity presented above.

Our results for this exercise are shown in table 2. Before we come to a detailed discussion

of these results, however, let us first present the remaining fits of table 1. As can be read off this table, the χ^2 of the K-matrix fits (6.10K1), (6.10K2), (6.11K1) and (6.11K2) is larger than 2 for all cases. Let us remark that this χ^2 only corresponds to the data points of [45] above 1.85 GeV, which have not yet been included in the fits (6.10) and (6.11), and the matching condition around 1.75 GeV. To improve the quality of our K-matrix fits, we have decided to include an additional term $b_{ij}s$ in the background. To maintain the required falloff of the T-matrix, for these fits the parameter $\kappa = 2$. In order to study the cutoff dependence we have performed this type of fits with the two values $c = 25$ GeV^2 and a lower cutoff $c = 4$ GeV^2.

For the fits (6.10K3), (6.10K4) and (6.11K4), we observe that the phase shifts at infinity turn out to be $\delta_{1\infty} = 2\pi$ and $\delta_{3\infty} = 0$. The reason for this change in the behaviour of the phase shifts lies in the fact that the second resonance couples almost equally to the first and the third channel, so that a small change in the fit parameters can shift the phase motion of π from the third to the first channel. For the parameter set where this happens, we also observe a vanishing inelasticity and thus zeros in the diagonal elements of the S-matrix. Therefore the phases $\delta_1(s)$ and $\delta_3(s)$ at this point become ambiguous, although their sum must be continuous (modulo 2π) since the matrix element S_{12} of eq. (3.9) is non-vanishing. As far as the phase shifts at infinity are concerned, the fit (6.11K3) behaves as (6.10K2) and (6.11K2). However, this fit displays an artificial rapid phase motion at an energy around 13 GeV, and although it has a rather good χ^2 and the results for $F_3(0)$ in table 2 turn out reasonable, we shall discard it in the following.

Our results for the absolute values of the form factors $F_1(s)$ and $F_3(s)$ in the case of the unitarised chiral plus K-matrix fits are shown in figures 5 and 6. The dotted lines represent the fits (6.10K1) and (6.11K1), the solid lines (6.10K2), (6.10K3) and (6.10K4), and finally, the dashed lines correspond to (6.11K2) and (6.11K4). Since all form factors for these fits are rather similar we have not tried to discriminate the curves further. Nevertheless, for $|F_3(s)|$, like in figure 3, there are differences in the form factor between the fit (6.10) and (6.11) which are most prominent around 1.2 GeV. These differences can already be seen in the T-matrix and they tend us to consider the fit (6.10) more physical, as was already concluded in ref. [1].

We shall return now to a discussion of table 2. In figures 7 and 8, we display $|F_1(s)|$ and $|F_3(s)|$ for our fits (6.10K3) and (6.10K4), while varying $F_1(\Delta_{K\pi})$. The dotted lines correspond to $F_1(\Delta_{K\pi}) = 1.21$, the solid lines to 1.22, and the dashed lines to 1.23. The curves which are higher at the $K_0^*(1430)$ resonance always represent the fit (6.10K4). As can be seen from table 2, for smaller values of $F_1(\Delta_{K\pi})$, $F_3(0)$ comes out larger and vice

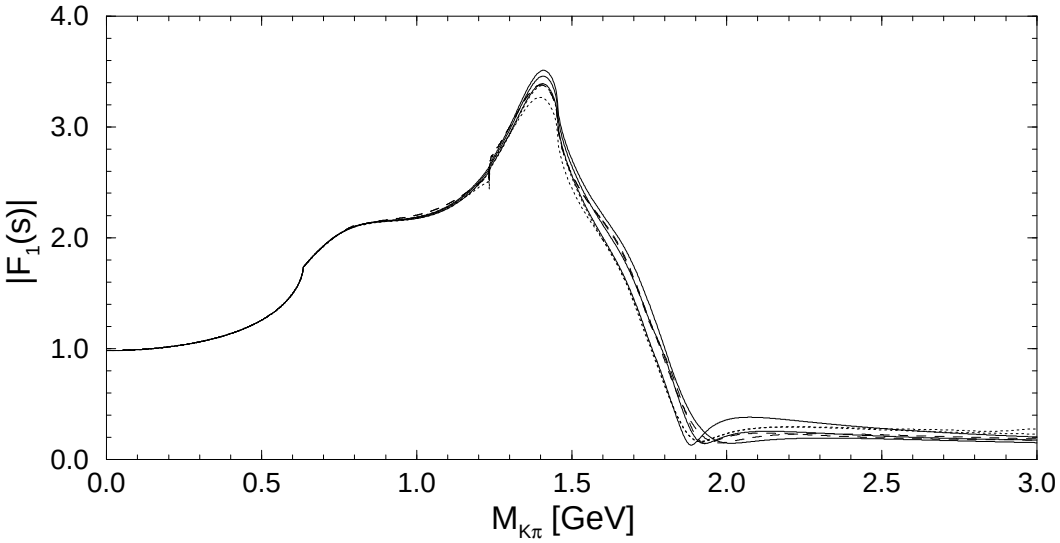

Figure 5: $|F_1(s)|$ in the two–channel case with K-matrix ansatz. The dotted lines correspond to the fits (6.10K1) and (6.11K1), the solid lines to (6.10K2), (6.10K3) and (6.10K4), and the dashed lines to (6.11K2) and (6.11K4).

versa. Averaging our results for the K-matrix fits, for $F_3(0)$ we then extract

$$F_{K\eta'}(0) \;=\; 0.58 \pm 0.04\,. \tag{4.6}$$

As the uncertainty we have chosen the maximal variation for the fits K3 and K4 with the better χ^2. The slightly larger variations in the case of K2, to our minds are due to the worse description of the experimental data. Also the derivative of the form factor $F_1(s)$ at zero, $D_1(0)$, comes out completely consistent with our expectation from χPT, with some variation for the fit (6.11K3), which anyway has been discarded for other reasons, although even this variation stays within the uncertainties. Finally, it is worth to note here that the predicted values for $F_3(0)$ from the fits (6.10K1) and (6.11K1) are in perfect agreement with the previous central value of $F_3(0)$, and their difference is completely accounted for by the estimated error in eq. (4.6).

4.3 The three–channel case

In the following, we investigate the solutions of the dispersion relations (B.1) in the full three–channel case for our unitarised chiral fits (6.10) and (6.11) of ref. [1]. In the three–channel case, we have not improved our fits in the region of the second resonance, because on the one hand just from the $K\pi$ scattering data there is not enough information to fit all parameters of a three-channel K-matrix, and, on the other hand, as was already mentioned

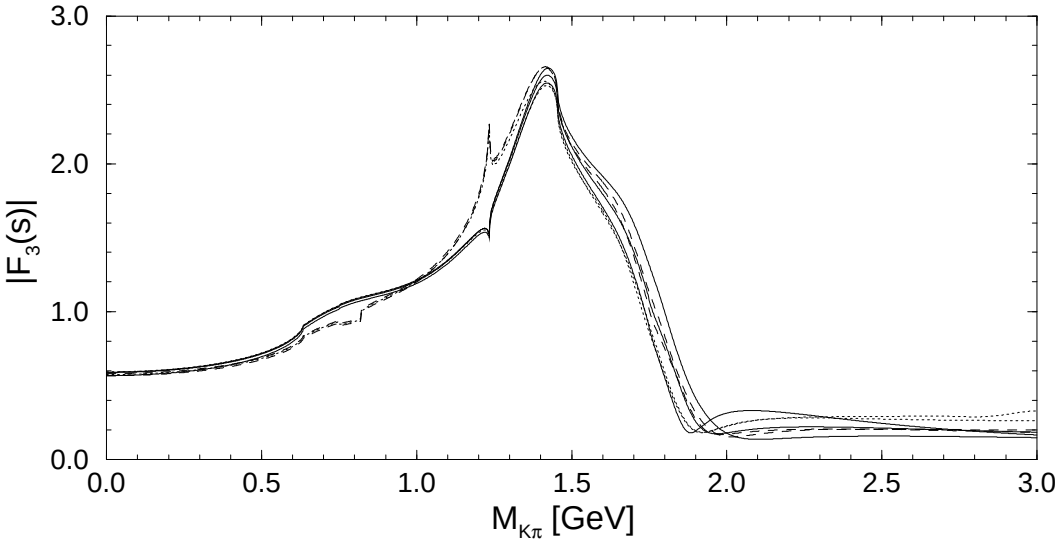

Figure 6: $|F_3(s)|$ in the two–channel case with K-matrix ansatz. The dotted lines correspond to the fits (6.10K1) and (6.11K1), the solid lines to (6.10K2), (6.10K3) and (6.10K4), and the dashed lines to (6.11K2) and (6.11K4).

above, the effects of the $K\eta$ channel will turn out so small that the more elaborate two–channel analysis with only $K\pi$ and $K\eta'$ for our purposes is completely sufficient.[4] As we shall verify below, this also entails that the form factors $F_1(s)$ and $F_3(s)$ are completely stable under the inclusion of the scalar $K\eta$ form factor $F_2(s)$. Therefore, this form factor will play a negligible role in the determination of the mass of the strange quark [52].

The numerical solution of the dispersion relations proceeds along the same lines as was already discussed in the last section for the two–channel case. Again, as initial functions for the form factors we can take the Omnès solution for $F_1^{(0)}(s)$, whereas the form factors $F_2^{(0)}(s)$ and $F_3^{(0)}(s)$ can be set to zero. Nevertheless, in order to prove the stability of the two–channel solutions (6.10) and (6.11) under the inclusion of the $K\eta$ channel, we have also used these solutions as initial functions $F_1^{(0)}(s)$ and $F_3^{(0)}(s)$ in the present three–channel case. Then the solution of the dispersion relations are iterated, until the procedure has converged and the form factors $F_1(s)$, $F_2(s)$ and $F_3(s)$ can be extracted. Of course, with both choices, the same final form factors are obtained.

In figure 9, we display the absolute values of the form factor $F_1(s)$ for the three–channel

[4]We have not taken into account the fit (6.7) of ref. [1], because when the $K\eta$ channel is removed for this fit, the χ^2 becomes rather large, increasing by almost a factor of two. On the theoretical side, this fit does not fullfill the short distance constraints presented in section 2. The strong sensitivity of the fit (6.7) on the $K\eta$ channel, and also the very small value of c_m, tend us to disregard this fit for further analysis.

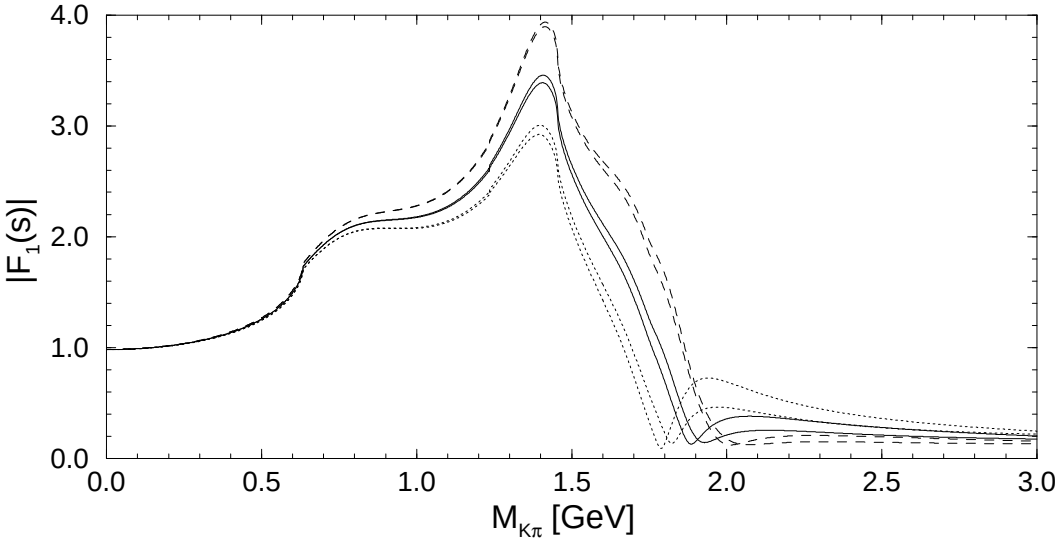

Figure 7: $|F_1(s)|$ for the fits (6.10K3) and (6.10K4) while varying $F_1(\Delta_{K\pi})$. The dotted lines correspond to $F_1(\Delta_{K\pi}) = 1.21$, the solid lines to 1.22, and the dashed lines to 1.23. The curves which are higher at the $K_0^*(1430)$ resonance always correspond to (6.10K4).

fits (6.10) and (6.11) of ref. [1], and in figure 10 the corresponding form factors $|F_2(s)|$ and $|F_3(s)|$ are shown. Like in section 4.2, the notation of the lines is (6.10) solid line and (6.11) long-dashed line. The three–channel form factors are plotted as thick lines and for comparison, in addition, as the thin lines we have displayed the two–channel form factors for the fits (6.10) and (6.11). In figure 10, the two lower lines correspond to $|F_2(s)|$. As can be observed from this figure, the form factors $F_2(s)$ turns out much smaller than $F_3(s)$, and for the scalar spectral function, further discussed in [52], it will be completely negligible. Furthermore, the two– and three–channel form factors are found to be very similar which again supports the finding that the $K\eta$ channel is rather unimportant.

Like in the case of the fits (6.10) and (6.11) for two channels, there is only one solution to the dispersion relations and we just have the freedom to fix the normalisation $F_1(0)$. The form factors $F_2(0)$ and $F_3(0)$ are then determined from the dispersion relation. The results for our three–channel fits are given by:

$$\begin{aligned} F_2^{(6.10)}(0) &= -0.195\,, & F_3^{(6.10)}(0) &= 0.426\,, \\ F_2^{(6.11)}(0) &= -0.269\,, & F_3^{(6.11)}(0) &= 0.424\,. \end{aligned} \tag{4.7}$$

As can already be guessed from the similarity of the two– and three–channel form factors, $F_3(0)$ for the fits (6.10) and (6.11) comes out very close to the corresponding numbers in the two–channel case. The result for $F_2(0)$ should be compared with the tree–level

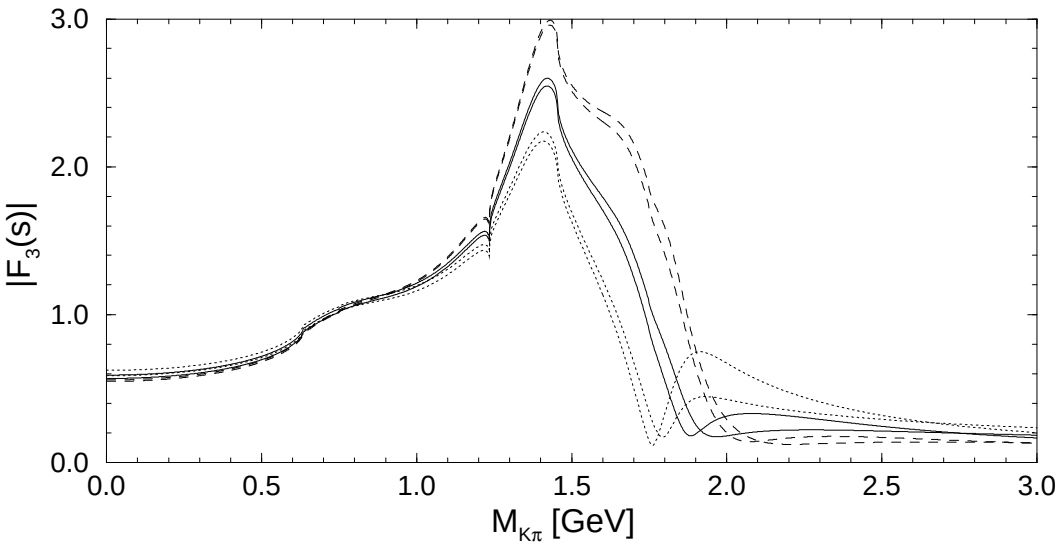

Figure 8: $|F_3(s)|$ for the fits (6.10K3) and (6.10K4) while varying $F_1(\Delta_{K\pi})$. The dotted lines correspond to $F_1(\Delta_{K\pi}) = 1.21$, the solid lines to 1.22, and the dashed lines to 1.23. The curves which are higher at the $K_0^*(1430)$ resonance always correspond to (6.10K4).

expectation from $\mathrm{U}(3)_L{\times}\mathrm{U}(3)_R$ χPT in the large-N_c limit including resonances, $F_2^{\chi\mathrm{PT}}(0) = -f_{K\eta}(0)/3 = -0.109$. Here for (6.11) the deviation amounts to more than a factor of two, and for (6.10) it is somewhat smaller. However, this difference is similar to that of $F_3(0)$ before improving the high energy tail of the experimental data above 1.75 GeV, and hence, until such an improvement is performed for the three-channel case, one cannot draw a definite conclusion on $F_2(0)$.

Like in the two–channel case, also for the three–channel fits (6.10) and (6.11) we investigate the low-energy constraints $F_1(\Delta_{K\pi})$, as well as the derivative of $F_1(s)$ at zero $D_1(0)$. The results are found as:

$$\begin{aligned} F_1^{(6.10)}(\Delta_{K\pi}) &= 1.266\,, & D_1^{(6.10)}(0) &= 0.927\,, \\ F_1^{(6.11)}(\Delta_{K\pi}) &= 1.264\,, & D_1^{(6.11)}(0) &= 0.909\,. \end{aligned} \tag{4.8}$$

Again, $F_1(\Delta_{K\pi})$ for three channels turns out very close to the two–channel case where also $F_1(\Delta_{K\pi})$ has been found too large, so that the corresponding form factors cannot be considered physical. Nevertheless, the finding that for both fits $F_1(\Delta_{K\pi})$ is very close is reflected in the fact that the full form factors $F_1(s)$ turn out very similar. The derivative of $F_1(s)$ at zero $D_1(0)$ for (6.10) and (6.11), on the other hand, also is close to the corresponding numbers in the two–channel case, as well as to the χPT expectation.

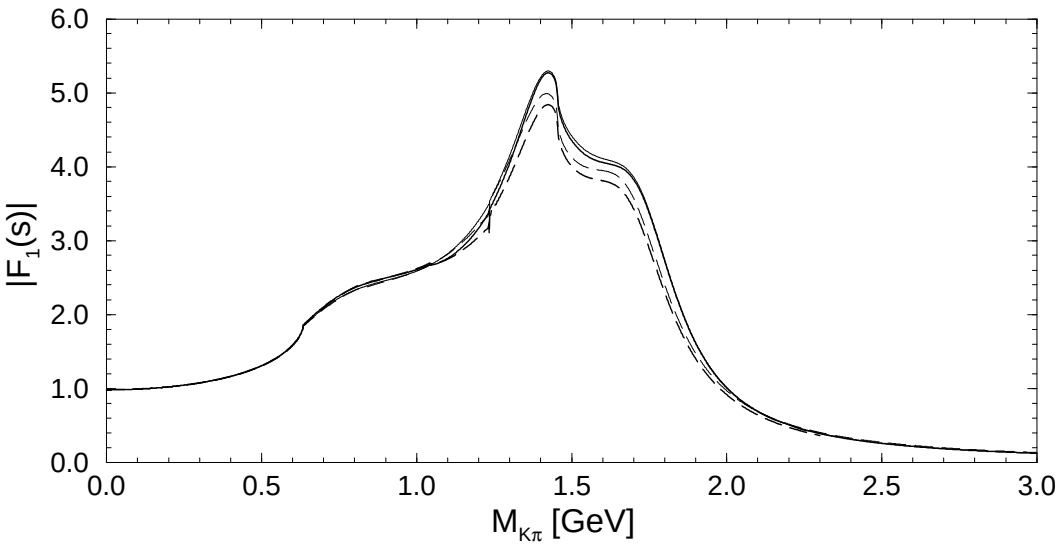

Figure 9: $|F_1(s)|$ in the three–channel case. The thick solid and long–dashed lines correspond to the unitarised χPT fits of eqs. (6.10) and (6.11) of [1] respectively. For comparison, as the thin lines we have also displayed the corresponding two–channel form factors for (6.10) and (6.11).

5 Conclusions

In this work, we have investigated the strangeness–changing scalar form factors for the $K\pi$, $K\eta$ and $K\eta'$ systems up to 2 GeV. To this end, first theoretical expressions for the scalar form factors were derived in the framework of the chiral Lagrangian including resonances in the limit of a large number of colours. In a second step, analyticity and unitarity constraints were employed to write down a set of dispersion relations for the form factors. Taking into account previous results on S–wave $K\pi$ scattering [1], the scalar $K\pi$, $K\eta$ and $K\eta'$ form factors could be extracted from the solutions of the coupled–channel dispersion relations.

The η and η' mesons can be described in the $\mathrm{U}(3)_L\times\mathrm{U}(3)_R$ effective theory in the large-N_c limit. In this framework, theoretical expressions for the tree–level scalar form factors have been derived in section 2. However, the couplings of the scalar meson resonances to the pseudoscalar mesons, c_d and c_m, which appear in the resonance chiral Lagrangian are not very well know. Assuming the scalar form factors to vanish at infinity, constraints on the scalar couplings could be obtained which are compatible with present phenomenological knowledge on c_d and c_m. In particular, if the chiral low-energy constants L_5 and L_8 are saturated by the scalar meson resonances, we deduced the relation $L_5 = 2L_8$, independent

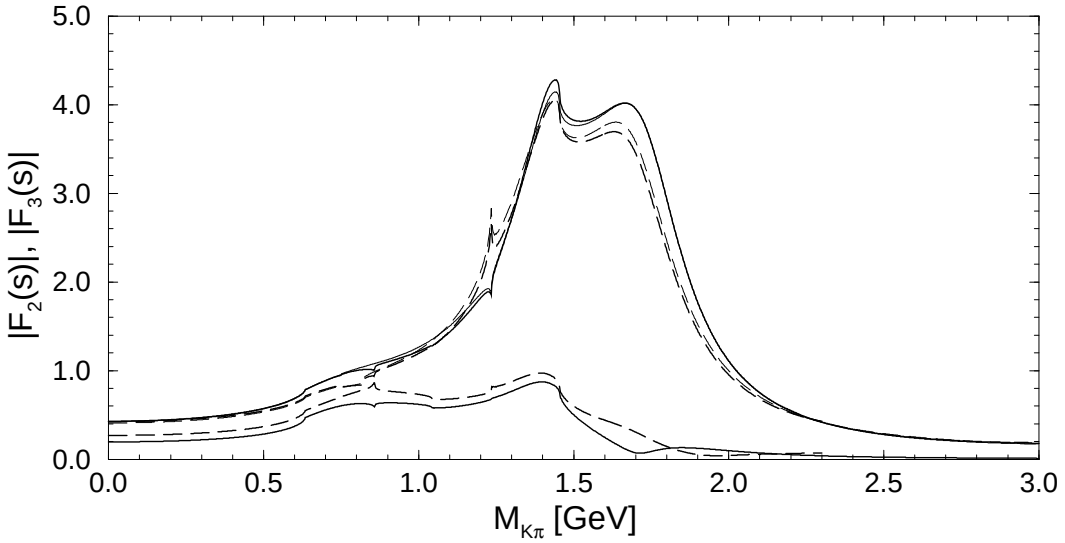

Figure 10: $|F_2(s)|$ and $|F_3(s)|$ in the three–channel case. The solid and long–dashed lines correspond to the unitarised χPT fits of eqs. (6.10) and (6.11) of [1] respectively. The two lower lines correspond to $|F_2(s)|$. For comparison, as the thin lines we have also displayed the corresponding two–channel form factors for (6.10) and (6.11).

of the number of resonances. Further consequences of the theoretical constraints have already been investigated in our previous analysis of S–wave $K\pi$ scattering [1], and in more detail in section 2.2. Furthermore, in the chiral framework it was found that the $K\eta$ form factor is strongly suppressed compared to the $K\pi$ and $K\eta'$ form factors.

Using unitarity and analyticity, we were able to write down a set of coupled dispersion relations, which relate the scalar form factors to the S–wave, isospin 1/2 scattering amplitude. In the elastic, single–channel case, an analytical solution of the dispersion relation due to Omnès is known, which only depends on the elastic S–wave phase shift. In the coupled–channel case the set of integral equations had to be solved numerically. To perform this step, an efficient algorithm to perform the Cauchy principal value integrals was developed, which is described in appendix C.2.

Using our results for different fits to the elastic $K\pi$ scattering data [1], it was found that the scalar $K\pi$ form factor $F_1(s)$ is not well determined in the single channel case and that higher energy data, as well as inelastic channels have to be included for a better description. Since it was shown that the $K\eta$ channel is suppressed, we have concentrated our detailed investigation of the form factors on the two–channel case with $K\pi$ and $K\eta'$. In general, the two–channel dispersion relations admit two linearly independent solutions, and thus we need two integration constants to fix them unambiguously.

An obvious choice for the first constant is $F_1(0)$ which is very well known from next-to-leading order χPT. Different possible choices for the second constant could be $F_3(0)$, the derivative of $F_1(s)$ at zero $D_1(0)$, or $F_1(\Delta_{K\pi})$ at the so-called Callan-Treiman point. We have used the last constraint because in our opinion it is known most precisely also from next-to-leading order χPT. With this information we then deduced $F_3(0) = 0.58 \pm 0.04$, compatible with the tree–level χPT expectation in the large-N_c limit. Furthermore, $F_3(0)$ is also in excellent agreement to the value from those fits with an improved high energy behaviour that gave rise to only one independent solution of the form factors.

The three–channel case was used to corroborate that indeed the $K\eta$ form factor $F_2(s)$ turns out much smaller than $F_1(s)$ and $F_3(s)$, and that the scalar $K\pi$ and $K\eta'$ form factors were practically unchanged compared to the two–channel case. This gives us confidence that the more elaborate two–channel analysis is sufficient for our purpose of determining the strangeness–changing scalar spectral function since the $K\eta$ contribution is negligible.

In a forthcoming work [52], our results for the scalar $K\pi$ and $K\eta'$ form factors will be utilised to explicitly calculate the corresponding strangeness–changing scalar spectral function up to 2 GeV. This spectral function is a key ingredient in the determination of the strange quark mass from QCD sum rules for the scalar correlator and it is also important in the corresponding analysis of the Cabibbo–suppressed hadronic τ decay width.

Acknowledgements

This work has been supported in part by the German–Spanish Cooperation Agreement HA97-0061, by the European Union TMR Network EURODAPHNE (ERBFMX-CT98-0169), and by DGESIC (Spain) under the grant no. PB97-1261 and DGICYT contract no. BFM2000-1326. M.J. would like to thank the Deutsche Forschungsgemeinschaft for support.

Appendices

A Loop functions

For completeness, we tabulate here the one-loop function $\bar{J}_{PQ}(s)$ [4] appearing in the next-to-leading order chiral form factors of eqs. (2.7) and (2.8):

$$\begin{aligned}\bar{J}_{PQ}(s) &\equiv -\frac{1}{16\pi^2}\int_0^1 dx\,\ln\left[\frac{M_P^2 - sx(1-x) - \Delta_{PQ}x}{M_P^2 - \Delta_{PQ}x}\right] \\ &= \frac{1}{32\pi^2}\left\{2 + \left(\frac{\Delta_{PQ}}{s} - \frac{\Sigma_{PQ}}{\Delta_{PQ}}\right)\ln\left(\frac{M_Q^2}{M_P^2}\right) - \frac{\lambda_{PQ}}{s}\ln\left[\frac{(s+\lambda_{PQ})^2 - \Delta_{PQ}^2}{(s-\lambda_{PQ})^2 - \Delta_{PQ}^2}\right]\right\},\end{aligned} \tag{A.1}$$

with

$$\Sigma_{PQ} \equiv M_P^2 + M_Q^2\,; \quad \Delta_{PQ} \equiv M_P^2 - M_Q^2\,; \quad \lambda_{PQ}^2 \equiv \left[s - (M_P + M_Q)^2\right]\left[s - (M_P - M_Q)^2\right]\,.$$

B Three–channel dispersion relations

Below we present the dispersion relations for the scalar form factors $F_k(s)$ in the full three–channel case including $K\pi$, $K\eta$ and $K\eta'$:

$$\begin{aligned}F_1(s) &= \frac{1}{\pi}\int_{s_{th\,1}}^{\infty} ds'\,\frac{\sigma_1(s')F_1(s')\,t_0^{11}(s')^*}{(s'-s-i0)} + \frac{1}{\pi}\int_{s_{th\,2}}^{\infty} ds'\,\frac{\sigma_2(s')F_2(s')\,t_0^{12}(s')^*}{(s'-s-i0)} \\ &+ \frac{1}{\pi}\int_{s_{th\,3}}^{\infty} ds'\,\frac{\sigma_3(s')F_3(s')\,t_0^{13}(s')^*}{(s'-s-i0)}\,, \\ F_2(s) &= \frac{1}{\pi}\int_{s_{th\,1}}^{\infty} ds'\,\frac{\sigma_1(s')F_1(s')\,t_0^{12}(s')^*}{(s'-s-i0)} + \frac{1}{\pi}\int_{s_{th\,2}}^{\infty} ds'\,\frac{\sigma_2(s')F_2(s')\,t_0^{22}(s')^*}{(s'-s-i0)} \\ &+ \frac{1}{\pi}\int_{s_{th\,3}}^{\infty} ds'\,\frac{\sigma_3(s')F_3(s')\,t_0^{23}(s')^*}{(s'-s-i0)}\,, \\ F_3(s) &= \frac{1}{\pi}\int_{s_{th\,1}}^{\infty} ds'\,\frac{\sigma_1(s')F_1(s')\,t_0^{13}(s')^*}{(s'-s-i0)} + \frac{1}{\pi}\int_{s_{th\,2}}^{\infty} ds'\,\frac{\sigma_2(s')F_2(s')\,t_0^{23}(s')^*}{(s'-s-i0)} \\ &+ \frac{1}{\pi}\int_{s_{th\,3}}^{\infty} ds'\,\frac{\sigma_3(s')F_3(s')\,t_0^{33}(s')^*}{(s'-s-i0)}\,.\end{aligned} \tag{B.1}$$

C Numerical solution of the dispersion relation

To illustrate our method for the numerical solution of the dispersion relation, below we shall discuss the single channel case. The coupled channel case can be treated in a completely analogous fashion.

C.1 Single channel case

In the single channel case, the dispersion relation reads:

$$\mathrm{Re}F_1(s) \;=\; \mathcal{P}\!\int_{s_{th}}^{\infty} ds'\,\frac{f_1(s')}{(s'-s)} \;=\; \mathcal{P}\!\int_{s_{th}}^{s_{cut}} ds'\,\frac{f_1(s')}{(s'-s)} + \mathcal{P}\!\int_{s_{cut}}^{\infty} ds'\,\frac{f_1(s')}{(s'-s)}\,, \tag{C.1}$$

with

$$f_1(s') \;\equiv\; \frac{1}{\pi}\,\mathrm{Im}F_1(s') \;=\; \frac{1}{\pi}\,\sigma_1(s')F_1(s')\,t_0^{11}(s')^*\,, \tag{C.2}$$

and $s_{th} = (M_K + M_\pi)^2$. For numerical purposes on the right-hand side we have split the integration range at an energy s_{cut}. Equation (C.1) can also be written as a once subtracted dispersion relation:

$$\mathrm{Re}F_1(s) \;=\; \int_{s_{th}}^{\infty} ds'\,\frac{f_1(s')}{s'} + \mathcal{P}\!\int_{s_{th}}^{\infty} ds'\,\frac{s f_1(s')}{s'(s'-s)}\,. \tag{C.3}$$

Assuming that $f_1(s)$ vanishes for $s \to \infty$, such that the first integral converges, it can be identified with $F_1(0)$. In the numerical analysis, we have also investigated solving the subtracted dispersion relation imposing $F_1(0)$ as a boundary condition.

For the numerical integration, it is convenient to perform a change of variables such that the integration range becomes finite. We shall transform both energy intervals to the interval $(0,1)$. For the low-energy interval (s_{th}, s_{cut}) a convenient transformation is:

$$s' \;\equiv\; s_{th} + (s_{cut} - s_{th})\,x'^2\,; \qquad x' \;=\; \sqrt{\frac{(s'-s_{th})}{(s_{cut}-s_{th})}}\,, \tag{C.4}$$

whereas for the high-energy region (s_{cut}, ∞) we chose:

$$s' \;\equiv\; s_{th}\,\frac{(1-b\,z')}{(1-z')}\,; \qquad z' \;=\; \frac{(s'-s_{th})}{(s'-b\,s_{th})}\,. \tag{C.5}$$

The additional parameter $b < 1$ in the second transformation has been introduced to allow for increasing the convergence of the method or to check the stability of the solution.

Defining the additional variables $x \equiv \sqrt{(s - s_{th})/(s_{cut} - s_{th})}$ and $z \equiv (s - s_{th})/(s - b\, s_{th})$, the unsubtracted dispersion relation takes the form:

$$\mathrm{Re}F_1(x) \;=\; \mathcal{P}\!\int_0^1 dx' \,\frac{2x' f_1(x')}{(x'^2 - x^2)} + \mathcal{P}\!\int_0^1 dz' \,\frac{(1-z) f_1(z')}{(1-z')(z'-z)}\,, \tag{C.6}$$

whereas the subtracted dispersion relation is given by:

$$\mathrm{Re}F_1(x) \;=\; F_1(0) + \mathcal{P}\!\int_0^1 dx' \,\frac{2x'[1+(a-1)x^2] f_1(x')}{[1+(a-1)x'^2](x'^2 - x^2)} + \mathcal{P}\!\int_0^1 dz' \,\frac{(1-bz) f_1(z')}{(1-bz')(z'-z)}\,, \tag{C.7}$$

with $a \equiv s_{cut}/s_{th}$. The additional factor of x' in the low-energy integral has the advantage of smoothing out the square-root singularity $x = x' = 0$.

As a further ingredient, for the iteration of the dispersion relation, we require a reasonably accurate numerical integration routine for the Cauchy principal value integrals. Generally, the most accurate integration routines are based on the Gauss algorithm. In the next section, we shall thus develop a Gauss algorithm for the Cauchy kernel.

C.2 Gauss quadrature for Cauchy kernel

Gaussian quadrature algorithms can be designed such that the approximation

$$\int_a^b f(y) w(y) dy \;\approx\; \sum_{j=1}^{N} w_j f(y_j) \tag{C.8}$$

is exact if $f(x)$ is a polynomial. The task for finding such algorithms is finding the set of weights w_j and abscissas y_j to accomplish this feat, given a weight function $w(y)$.

The starting point for developing the Gauss algorithm lies in finding a complete basis of functions which are orthogonal with respect to the weight function $w(y)$ [55]. For the trivial weight $w(y) = 1$, on the interval $(-1, 1)$, this set of functions can be chosen to be the Legendre polynomials $P_n(y)$ and the corresponding integration formula is the so-called Gauss–Legendre algorithm.

Defining the scalar product of two functions f and g over the weight function $w(y)$ as

$$\langle f|g\rangle \;=\; \int_a^b f(y) g(y) w(y) dy\,, \tag{C.9}$$

we therefore seek functions $u_n(y)$ such that $\langle u_m|u_n\rangle$ is zero if $m \neq n$. Choosing the Cauchy weight $w(y) = 1/(x - y)$, it can be shown that again on the interval $(-1, 1)$ a set of

orthogonal functions is given by

$$u_n(x,y) \;=\; P_n(y) - \frac{Q_n(x)}{Q_{n-1}(x)}\, P_{n-1}(y)\,, \tag{C.10}$$

where $Q_n(x)$ are the associated Legendre functions of the second kind [56]. The normalisation is easily found to be:

$$\langle u_n|u_n\rangle \;=\; 2\,Q_n(x)\Big[\, P_n(x) - \frac{Q_n(x)}{Q_{n-1}(x)}\, P_{n-1}(x)\,\Big] \;=\; 2\,Q_n(x)\,u(x,x)\,. \tag{C.11}$$

For a Gauss algorithm of order N, the set of abscissas is now given by the zeros y_j of the function $u_N(y)$ in the interval (a,b), and the weights w_j can be calculated from a general formula, which can for example be found in the Numerical Recipes [55]. In our particular case, however, we still have the complication that the weight function, and thus also the u_n, also depend on the additional variable x. The problem simplifies considerably, if we only evaluate our integral at the zeros x_i of the function $Q_N(x)$. Then our set of orthogonal functions is again the Legendre polynomials, and from a straightforward calculation, the weights $w_j(x_i)$ are obtained to be

$$w_j(x_i) \;=\; \frac{2(1-y_j^2)}{N(x_i-y_j)}\,\frac{Q_{N-1}(x_i)\,P_N(x_i)}{P_{N-1}^2(y_j)}\,. \tag{C.12}$$

Our final integration formula reads:

$$\int_{-1}^{1} f(y)\,\frac{dy}{(x_i-y)} \;=\; \sum_{j=1}^{N} w_j(x_i) f(y_j)\,. \tag{C.13}$$

It is a trivial matter to find the integration formula for a general interval (a,b) using linear transformations. The result for the integral at values of x different from x_i can be calculated with the help of standard interpolation algorithms [55]. A final comment concerns the practical calculation of the roots of Q_N. Once the N roots of P_N on the interval $(-1,1)$ are computed with a standard algorithm [55], the $N+1$ roots of Q_N are easily searched for, because the always interleave the roots of P_N.

Although the presented Gauss algorithm is rather simple, we were unable to find it in the literature. Thus, in appendix D we present our Fortran implementation of the algorithm which is based on the Gauss–Legendre algorithm given in the Numerical Recipes [55].

D Fortran code for the Gauss routine

```
C-----------------------------------------------------------------------
      !
C     ! Small program to test the subroutine "cauleg"
C     ! Calculates the integral int( sin(y)^2/(x-y), y=0:3);
C     ! Last change: 12.1.2001
C     ! Matthias Jamin: m.jamin@thphys.uni-heidelberg.de
      !
      Program CauLegTest
      Implicit Double Precision (A-z)
      Integer i, j, ngau
      Parameter (ngau = 63, a = 0.D0, b = 3.D0)
      Dimension x(ngau+1), y(ngau), w(ngau+1,ngau)
      !
C     ! Calculate zeros of the Legendre polynomials and Cauchy weights
      !
      Call cauleg(a,b,x,y,w,ngau)
      !
C     ! Calculate integral at the zeros x(i) of Q_n(x)
      !
      Open (unit=8, file='cauleg.out')
      Do 20 i=1,ngau+1
      !
      sum = 0.D0
      Do 10 j=1,ngau
   10 sum = sum + dsin(y(j))**2*w(i,j)
      si1 = sum
      !
C     ! With the CERN library "mathlib" this is the exact result
      !
      xx = x(i)
      si2 = ( dcos(2.D0*xx)*(dcosin(2.D0*(a-xx))-dcosin(2.D0*(b-xx)))
     .      + dsin(2.D0*xx)*(dsinin(2.D0*(xx-a))-dsinin(2.D0*(xx-b)))
     .      + dlog((b-xx)/(xx-a)) )/2.D0
      !
   20 Write (8,*) x(i), si1, si2
      Close (8)
      !
      Return
      End
```

```
C-----------------------------------------------------------------------
      !
C     ! Gauss routine for integration with the Cauchy kernel 1/(x-y)
C     ! based on the routine "gauleg" from the Numerical Recipes.
C     ! Uses legp(x,n) and legq(x,n)
      !
C     ! Given the lower and upper limits of integration x1 and x2, and
C     ! given n, the routine returns arrays x(1:n+1), y(1:n), w(1:n+1,1:n)
C     ! containing the points x where the integral should be evaluated,
C     ! as well as the abscissas and the weights of the Gauss-Legendre
C     ! n-point quadrature formula. x(1:n+1) and y(1:n) contain the roots
C     ! of the Legendre functions Q_n and P_n of order n, shifted to the
C     ! interval (x1,x2). Other values of x have to be calculated with
C     ! standard interpolation methods.
      !
      Subroutine cauleg(x1,x2,x,y,w,n)
      Implicit Double Precision (A-z)
      Integer i, j, m, n
      Dimension x(n+1), y(n), w(n+1,n)
      Parameter (Pi = 3.141592653589793238D0, eps = 1.D-15)
      !
      m = (n+1)/2
      xm = 0.5D0*(x2+x1)
      xl = 0.5D0*(x2-x1)
      !
      Do 20 i=1,m
         z = dcos(Pi*(i-0.25D0)/(n+0.5D0))
   10    z1 = z
         Call legp(p1,pp,z,n)
         z = z1-p1/pp
         If (dabs(z-z1).gt.eps) Goto 10
         y(i) =     xm-xl*z
         y(n-i+1) = xm+xl*z
   20 Continue
      !
      Do 40 i=1,m+1
         If (i.eq.1) Then
            z = -1.D0+1.D-9
         Else
            z = 0.5D0*(y(i)+y(i-1)-2.D0*xm)/xl
         End If
   30    z1 = z
         Call legq(q1,qp,z,n)
```

```
         z = z1-q1/qp
         If (dabs(z-z1).gt.eps) Goto 30
         x(i) =     xm+xl*z
         x(n-i+2) = xm-xl*z
   40 Continue
      !
      Do 50 i=1,m+1
         xi = (x(i)-xm)/xl
         Call legp(p1,pp,xi,n)
         Call legq(q2,qp,xi,n-1)
         Do 50 j=1,n
            yj = (y(j)-xm)/xl
            Call legp(p2,pp,yj,n-1)
            w(i,j) = 2.D0/dble(n)*(1.D0-yj*yj)
     .               /(yj-xi)*p1*q2/p2/p2
            w(n-i+2,n-j+1) = -w(i,j)
   50 Continue
      !
      Return
      End
C-----------------------------------------------------------------------
      !
C     ! Calculates the Legendre polynomials P_n(x) and P'_n(x)
C     ! P_n(x) is in p1 and P'_n(x) in pp.
      !
      Subroutine legp(p1,pp,x,n)
      Implicit Double Precision (A-z)
      Integer j, n
      !
      p2 = 1.D0
      p1 = x
      Do 10 j=2,n
         p3 = p2
         p2 = p1
         p1 = ((2.D0*j-1.D0)*x*p2-(j-1.D0)*p3)/j
   10 Continue
      pp = n*(x*p1-p2)/(x*x-1.D0)
      !
      Return
      End
C-----------------------------------------------------------------------
      !
C     ! Calculates the Legendre functions Q_n(x) and Q'_n(x).
```

```
C     ! Q_n(x) is in q1 and Q'_n(x) in qp.
      !
      Subroutine legq(q1,qp,x,n)
      Implicit Double Precision (A-z)
      Integer j, n
      !
      q2 = 0.5D0*dlog(dabs((1.D0+x)/(1.D0-x)))
      q1 = x*q2-1.D0
      Do 10 j=2,n
         q3 = q2
         q2 = q1
         q1 = ((2.D0*j-1.D0)*x*q2-(j-1.D0)*q3)/j
   10 Continue
      qp = n*(x*q1-q2)/(x*x-1.D0)
      !
      Return
      End
C-------------------------------------------------------------------------
```

References

[1] M. Jamin, J. A. Oller, and A. Pich, S-wave $K\pi$ scattering in chiral perturbation theory with resonances, *Nucl. Phys.* **B587** (2000) 331.

[2] S. Weinberg, Phenomenological Lagrangians, *Physica* **A96** (1979) 327.

[3] J. Gasser and H. Leutwyler, Chiral perturbation theory to one loop, *Ann. Phys.* **158** (1984) 142.

[4] J. Gasser and H. Leutwyler, Chiral perturbation theory: expansions in the mass of the strange quark, *Nucl. Phys.* **B250** (1985) 465, 517, 539.

[5] G. Ecker, Low-energy QCD, *Prog. Part. Nucl. Phys.* **36** (1996) 71.

[6] A. Pich, Chiral perturbation theory, *Rept. Prog. Phys.* **58** (1995) 563.

[7] U.-G. Meissner, Recent developments in chiral perturbation theory, *Rept. Prog. Phys.* **56** (1993) 903.

[8] G. Ecker, J. Gasser, A. Pich, and E. de Rafael, The role of resonances in chiral perturbation theory, *Nucl. Phys.* **B321** (1989) 311.

[9] G. Ecker, J. Gasser, H. Leutwyler, A. Pich, and E. de Rafael, Chiral Lagrangians for massive spin 1 fields, *Phys. Lett.* **B223** (1989) 425.

[10] G. 't Hooft, A planar diagram theory for strong interactions, *Nucl. Phys.* **B72** (1974) 461.

[11] E. Witten, Baryons in the $1/N_c$ expansion, *Nucl. Phys.* **B160** (1979) 57.

[12] S. Peris, M. Perrottet, and E. de Rafael, Matching long and short distances in large-N_c QCD, *JHEP* **05** (1998) 011.

[13] S. Narison, N. Paver, E. de Rafael, and D. Treleani, Light quark mass differences in quantum chromodynamics, *Nucl. Phys.* **B212** (1983) 365.

[14] M. Jamin and M. Münz, The Strange quark mass from QCD sum rules, *Z. Phys.* **C66** (1995) 633.

[15] K. G. Chetyrkin, C. A. Dominguez, D. Pirjol, and K. Schilcher, Mass singularities in light quark correlators: the strange quark case, *Phys. Rev.* **D51** (1995) 5090.

[16] K. G. Chetyrkin, D. Pirjol, and K. Schilcher, Order α_s^3 determination of the strange quark mass, *Phys. Lett.* **B404** (1997) 337.

[17] P. Colangelo, F. de Fazio, G. Nardulli, and N. Paver, On the QCD sum rule determination of the strange quark mass, *Phys. Lett.* **B408** (1997) 340.

[18] M. Jamin, The strange quark mass from scalar sum rules updated, *Nucl. Phys. Proc. Suppl.* **64** (1998) 250, Proc. of *QCD 97*, Montpellier, July 1997.

[19] T. Bhattacharya, R. Gupta, and K. Maltman, Duality and the extraction of light quark masses from finite energy and QCD sum rules, *Phys. Rev.* **D57** (1998) 5455.

[20] K. Maltman, The strange quark mass from finite energy sum rules, *Phys. Lett.* **B462** (1999) 195.

[21] A. Pich and J. Prades, Perturbative quark mass corrections to the τ hadronic width, *JHEP* **06** (1998) 013.

[22] ALEPH collaboration, Study of τ decays involving kaons, spectral functions and determination of the strange quark mass, *Eur. Phys. J.* **C11** (1999) 599.

[23] A. Pich and J. Prades, Strange quark mass determination from Cabibbo-suppressed τ decays, *JHEP* **10** (1999) 004.

[24] J. G. Körner, F. Krajewski, and A. A. Pivovarov, Determination of the strange quark mass from Cabibbo suppressed tau decays with resummed perturbation theory in an effective scheme, *Eur. Phys. J.* **C20** (2001) 259.

[25] J. Kambor and K. Maltman, The strange quark mass from flavor breaking in hadronic τ decays, *Phys. Rev.* **D62** (2000) 093023.

[26] S. Chen, M. Davier, E. Gámiz, A. Höcker, A. Pich, *et al.*, Strange quark mass from the invariant mass distribution of Cabibbo-suppressed τ decays, (2001), hep-ph/0105253, to appear in *Eur. Phys. J.*

[27] T. N. Truong, Chiral perturbation theory and final state theorem, *Phys. Rev. Lett.* **61** (1988) 2526.

[28] A. Dobado, M. J. Herrero, and T. N. Truong, Unitarized chiral perturbation theory and elastic pion-pion scattering, *Phys. Lett.* **B235** (1990) 134.

[29] J. A. Oller and E. Oset, Chiral symmetry amplitudes in the S-wave isoscalar and isovector channels and the σ, $f_0(980)$, $a_0(980)$ scalar mesons, *Nucl. Phys.* **A620** (1997) 438, Erratum *Nucl. Phys.* **A652** (1999) 407.

[30] F. Guerrero and A. Pich, Effective field theory description of the pion form factor, *Phys. Lett.* **B412** (1997) 382.

[31] F. Guerrero, Study of the resummation of chiral logarithms in the exponentiated expression for the pion form factor, *Phys. Rev.* **D57** (1998) 4136.

[32] J. A. Oller, E. Oset, and J. R. Peláez, Meson-meson and meson-baryon interactions in a chiral non-perturbative approach, *Phys. Rev. Lett.* **80** (1998) 3452, *Phys. Rev.* **D59** (1999) 074001.

[33] J. A. Oller and E. Oset, N/D description of two-meson amplitudes and chiral symmetry, *Phys. Rev.* **D60** (1999) 074023.

[34] J. A. Oller, E. Oset, and A. Ramos, Chiral unitary approach to meson-meson and meson-baryon interactions and nuclear applications, *Prog. Part. Nucl. Phys.* **45** (2000) 157.

[35] D. Gómez Dumm, A. Pich, and J. Portoles, The hadronic off-shell width of meson resonances, *Phys. Rev.* **D62** (2000) 054014.

[36] U.-G. Meissner and J. A. Oller, $J/\psi \to \phi\pi\pi$ $(K\overline{K})$ decays, chiral dynamics and OZI violation, *Nucl. Phys.* **A679** (2001) 671.

[37] J. A. Oller, E. Oset, and J. E. Palomar, Pion and kaon vector form factors, *Phys. Rev.* **D63** (2001) 114009.

[38] A. Pich and J. Portoles, The vector form factor of the pion from unitarity and analyticity: A model-independent approach, *Phys. Rev.* **D63** (2001) 093005.

[39] J. A. Oller, The case of a WW dynamical scalar resonance within a chiral effective description of the strongly interacting Higgs sector, *Phys. Lett.* **B477** (2000) 187.

[40] H. Leutwyler, Bounds on the light quark masses, *Phys. Lett.* **B374** (1996) 163.

[41] P. Herrera-Siklódy, J. I. Latorre, P. Pascual, and J. Taron, Chiral effective Lagrangian in the large-N_c limit: the nonet case, *Nucl. Phys.* **B497** (1997) 345.

[42] P. Herrera-Siklódy, J. I. Latorre, P. Pascual, and J. Taron, η–η' mixing from $\mathrm{U}(3)_L \times \mathrm{U}(3)_R$ chiral perturbation theory, *Phys. Lett.* **B419** (1998) 326.

[43] G. Amoros, J. Bijnens, and P. Talavera, QCD isospin breaking in meson masses, decay constants and quark mass ratios, *Nucl. Phys.* **B602** (2001) 87.

[44] P. Estabrooks et al., Study of $K\pi$ scattering using the reactions $K^{\pm}p \to K^{\pm}\pi^{+}n$ and $K^{\pm}p \to K^{\pm}\pi^{-}\Delta^{++}$ at 13 GeV/c, *Nucl. Phys.* **B133** (1978) 490.

[45] D. Aston et al., A study of $K^{-}\pi^{+}$ scattering in the reaction $K^{-}p \to K^{-}\pi^{+}n$ at 11 GeV/c, *Nucl. Phys.* **B296** (1988) 493.

[46] K. M. Watson, Some general relations between the photoproduction and scattering of π mesons, *Phys. Rev.* **95** (1954) 228.

[47] O. Babelon, J.-L. Basdevant, D. Caillerie, and G. Mennessier, Unitarity and inelastic final state interactions, *Nucl. Phys.* **B113** (1976) 445.

[48] R. Omnès, On the Solution of certain singular integral equations of quantum field theory, *Nuovo Cim.* **8** (1958) 316.

[49] E. Pallante and A. Pich, Final state interactions in kaon decays, *Nucl. Phys.* **B592** (2001) 294.

[50] J. F. Donoghue, J. Gasser, and H. Leutwyler, The decay of a light Higgs boson, *Nucl. Phys.* **B343** (1990) 341.

[51] A. D. Martin and T. D. Spearman, *Elementary Particle Theory*, North-Holland, Amsterdam, 1970.

[52] M. Jamin, J. A. Oller, and A. Pich, Light quark masses from scalar sum rules, IFIC/01-52, hep-ph/0110194.

[53] F. James and M. Roos, 'MINUIT' a system for function minimization and analysis of the parameter errors and correlations, *Comput. Phys. Commun.* **10** (1975) 343.

[54] D. E. Groom et al., Review of particle physics, *Eur. Phys. J.* **C15** (2000) 1.

[55] W. H. Press et al., *Numerical Recipes*, Cambridge University Press, 1992.

[56] I. S. Gradshteyn and I. M. Ryzhik, *Tables of integrals, series, and products*, Academic Press, 1980.